



# Validation of the Gaia Early Data Release 3 Parallax Zero-point Model with Asteroseismology

Joel C. Zinn<sup>1</sup>

Department of Astrophysics, American Museum of Natural History, Central Park West at 79th Street, New York, NY 10024, USA; [jzinn@amnh.org](mailto:jzinn@amnh.org)  
Received 2021 January 18; revised 2021 February 13; accepted 2021 February 22; published 2021 April 8

## Abstract

Gaia Early Data Release 3 (EDR3) provides trigonometric parallaxes for 1.5 billion stars, with reduced systematics compared to Gaia Data Release 2 and reported precisions better by up to a factor of 2. New to EDR3 is a tentative model for correcting the parallaxes of magnitude-, position-, and color-dependent systematics for five- and six-parameter astrometric solutions,  $Z_5$  and  $Z_6$ . Using a sample of over 2000 first-ascent red giant branch stars with asteroseismic parallaxes, I perform an independent check of the  $Z_5$  model in a Gaia magnitude range of  $9 \lesssim G \lesssim 13$  and color range of  $1.4 \mu\text{m}^{-1} \lesssim \nu_{\text{eff}} \lesssim 1.5 \mu\text{m}^{-1}$ . This analysis therefore bridges the Gaia team’s consistency check of  $Z_5$  for  $G > 13$  and indications from independent analysis using Cepheids of a  $\approx 15 \mu\text{as}$  overcorrection for  $G < 11$ . I find overcorrection sets in at  $G \lesssim 10.8$ , such that  $Z_5$ -corrected EDR3 parallaxes are larger than asteroseismic parallaxes by  $15 \pm 3 \mu\text{as}$ . For  $G \gtrsim 10.8$ , EDR3 and asteroseismic parallaxes in the Kepler field agree up to a constant consistent with expected spatial variations in EDR3 parallaxes after a linear, color-dependent adjustment. I also infer an average underestimation of EDR3 parallax uncertainties in the sample of  $22\% \pm 6\%$ , consistent with the Gaia team’s estimates at similar magnitudes and independent analysis using wide binaries. Finally, I extend the Gaia team’s parallax spatial covariance model to brighter magnitudes ( $G < 13$ ) and smaller scales (down to  $\approx 0.1^\circ$ ), where systematic EDR3 parallax uncertainties are at least  $\approx 3\text{--}4 \mu\text{as}$ .

*Unified Astronomy Thesaurus concepts:* [Parallax \(1197\)](#); [Asteroseismology \(73\)](#); [Red giant stars \(1372\)](#); [Stellar distance \(1595\)](#)

## 1. Introduction

The Gaia mission has provided astrometric information for over 1.5 billion stars as part of Gaia Early Data Release 3 (EDR3), which is largely complete down to  $G \sim 21$  in uncrowded regions (Gaia Collaboration et al. 2012). This release successfully builds upon the previous Data Release 2 (DR2; Gaia Collaboration et al. 2016, 2018), with improvements to the mission’s angular resolution, completeness, and astrometric precision. In particular, the reported parallax precision in EDR3 has improved by a factor of 2 from  $\approx 40 \mu\text{as}$  for sources with  $G < 15$  to  $\approx 20 \mu\text{as}$ .

Because of the nominal increase in parallax precision, it is all the more important to understand systematic uncertainties in the Gaia parallaxes. Following indications of systematic errors in the Gaia Data Release 1 parallaxes from the Gaia team and from subsequent independent investigations (Michalik et al. 2015; De Ridder et al. 2016; Gaia Collaboration et al. 2016; Jao et al. 2016; Lindegren et al. 2016; Stassun & Torres 2016; Davies et al. 2017; Huber et al. 2017; Zinn et al. 2017), several studies investigated the Gaia zero point in Gaia DR2. Many of the studies investigated the level of the global offset, which is due to degeneracies between variations in the angular separation of the spacecraft’s fields of view and the parallax zero point of the astrometric solution (Butkevich et al. 2017; Lindegren et al. 2018). These studies required independent parallax estimates to compare the Gaia parallaxes against and ranged from independent trigonometric parallaxes (Leggett et al. 2018), classical Cepheid photometric parallaxes (Groenewegen 2018; Riess et al. 2018), RR Lyrae photometric parallaxes (Muraveva et al. 2018; Layden et al. 2019; Marconi et al. 2021), open cluster/OB association isochronal parallaxes

(Yalyalieva et al. 2018; Melnik & Dambis 2020; Sun et al. 2020), very long baseline interferometric parallaxes (Kounkel et al. 2018; Bobylev 2019), statistical parallaxes (Schönrich et al. 2019; Muhie et al. 2021), and red giant asteroseismic parallaxes (Hall et al. 2019; Khan et al. 2019).

Apart from the 10–100  $\mu\text{as}$  global offset inferred by the aforementioned studies, the Gaia team also identified position-, color- and magnitude-dependent trends in the Gaia zero point, which were thought to result from Gaia’s scanning pattern and CCD response (Arenou et al. 2018; Lindegren et al. 2018). Independent studies subsequently confirmed similar trends (Leung & Bovy 2019; Zinn et al. 2019a, 2019b; Chan & Bovy 2020; Fardal et al. 2021).

The global offset and position-, color-, and magnitude-dependent parallax systematics quantified in DR2 are also present, though to a lesser extent, in EDR3 (Lindegren et al. 2020a, 2020b). The reduction in systematics is a result of EDR3 benefitting from a new astrometric solution using 34 months of data as opposed to DR2’s 22 months; improvements in EDR3 to the Velocity error and effective Basic Angle Calibration (VBAC) model, which models the basic angle variations that contribute to the global offset component of the parallax zero point; as well as improvements in the photometric image parameter determination (Rowell et al. 2020) and its iterative inclusion in the astrometric solution (Lindegren et al. 2020b).

Whereas the Gaia team did not recommend a specific parallax zero-point correction in DR2, a model for the parallax zero point has been provided for EDR3. This model is fit according to an iterative solution based ultimately on a sample of quasars distributed across the sky (Lindegren et al. 2020a), for which the EDR3 parallaxes should be effectively zero. The resulting model, denoted  $Z_5$  or  $Z_6$ , depending on whether the

<sup>1</sup> NSF Astronomy and Astrophysics Postdoctoral Fellow.

parallax is from a five-parameter or six-parameter astrometric solution,<sup>2</sup> once subtracted from the raw EDR3 parallaxes, is meant to remove most magnitude-, color-, and position-dependent errors.

The Gaia team has checked the  $Z_5$  model using stars in the Large Magellanic Cloud (LMC), open cluster members, and wide binaries (Fabricius et al. 2020; Lindegren et al. 2020a), finding good performance across a range of magnitude and color parameter space.

Since the EDR3 release, independent analyses have begun to quantify what adjustments may be required of the  $Z_5$  model. Riess et al. (2021), using a sample of classical Cepheids ( $G \lesssim 11$ ,  $1.35 \mu\text{m}^{-1} \lesssim \nu_{\text{eff}} \lesssim 1.6 \mu\text{m}^{-1}$ ), infer an offset of  $-14 \pm 6 \mu\text{as}$  such that corrected Gaia parallaxes are larger than Cepheid photometric parallaxes. Bhardwaj et al. (2021), appealing to blue RR Lyrae ( $\nu_{\text{eff}} > 1.5 \mu\text{m}^{-1}$ ), find an offset with corrected Gaia parallaxes of  $-25 \pm 5 \mu\text{as}$  in the same direction. Stassun & Torres (2021), using 76 bright, blue eclipsing binaries ( $5 \lesssim G \lesssim 12$ ,  $\nu_{\text{eff}} > 1.5 \mu\text{m}^{-1}$ ), show no statistically significant parallax residuals after correction according to the Gaia parallax model ( $+15 \pm 18 \mu\text{as}$ ). Moreover, an analysis using photometric parallaxes of red clump stars has recently indicated parallax residuals for  $G < 10.8$  and as a function of ecliptic longitude (Huang et al. 2021).

There is, however, nearly a complete absence of stars with  $1.4 \mu\text{m}^{-1} < \nu_{\text{eff}} < 1.5 \mu\text{m}^{-1}$ ,  $G < 13$  in either the LMC sample used for validation of the  $Z_5$  solution (Lindegren et al. 2020a) or any of the independent validation test samples thus far. This range in magnitude space is especially interesting to explore given that it links the  $G > 13$  checks at similar colors with the LMC by the Gaia team to the  $G < 11$  study from Riess et al. (2021). I therefore consider in this paper the evidence for adjustments to the  $Z_5$  model by appealing to asteroseismic parallaxes of more than 2000 first-ascent red giant branch stars, which occupy this region of magnitude and color parameter space. Specifically, I look for errors in Gaia parallaxes corrected according to the Gaia  $Z_5$  parallax zero-point model as a function of color and magnitude. In so doing, I also consider the evidence for corrections to the formal statistical uncertainties in Gaia parallaxes, as well as evidence for spatially correlated uncertainties in Gaia parallaxes.

## 2. Data

Asteroseismic data are adopted from APOKASC-2 (Pinsonneault et al. 2018), which consists of asteroseismic parameters for red giant branch stars,  $\nu_{\text{max}}$  and  $\Delta\nu$ , derived from light curves acquired by the Kepler mission (Borucki et al. 2010), as well as spectroscopic temperatures and metallicities from the Apache Point Observatory Galactic Evolution Experiment (APOGEE; Majewski et al. 2010), a survey within Sloan Digital Sky Survey IV (Blanton et al. 2017). I also appeal to an independent analysis of Kepler data from Yu et al. (2018) using the SYD asteroseismic pipeline (Huber et al. 2009). Whereas the APOKASC-2 asteroseismic measurements are average measurements based on results from five asteroseismic pipelines, using

data from SYD alone provides a check on the sensitivity of the result to the asteroseismic data.

I make use of APOGEE DR16 (Ahumada et al. 2020) parameters in this work, updated from the APOGEE DR14 (Holtzman et al. 2018) parameters provided in Pinsonneault et al. (2018). Both APOGEE DR14 and DR16 data are taken using the  $R = 22,500$  APOGEE spectrograph on the 2.5 m telescope of the Sloan Digital Sky Survey (Gunn et al. 2006; Wilson et al. 2019). The data reduction pipeline for APOGEE is described in Nidever et al. (2015), and the spectroscopic analysis is performed using the APOGEE Stellar Parameter and Chemical Abundance Pipeline (ASPCAP; García Pérez et al. 2016). The APOGEE temperatures are calibrated to be on the infrared flux method scale of González Hernández & Bonifacio (2009; Holtzman et al. 2015), which, for the red giant sample I work with here, implies temperatures are on an absolute scale to within  $\approx 20$  K (Zinn et al. 2019b); I adopt statistical uncertainties of 30 K.

I cross-matched the APOKASC-2 sample with EDR3 by first matching the APOKASC-2 stars to Gaia DR2 sources using the DR2-2MASS cross-match (Marrese et al. 2019), and then using the Gaia DR2 designations to match to EDR3 sources using the EDR3-DR2 cross-match (Torra et al. 2020). In so doing, I only kept stars that have angular separations between DR2 and EDR3 sources of less than 100 mas.

Most of the APOKASC-2 stars have five-parameter solutions instead of six-parameter solutions (44 versus 2130 first-ascent red giant branch stars after quality cuts), so the following analysis only uses stars with five-parameter astrometry solutions and thus concentrates on the validation of the  $Z_5$  model.

To ensure that the astrometric solutions are not affected by binarity, I followed the quality cuts of Fabricius et al. (2020), rejecting stars with  $\text{ruwe} \geq 1.4$ ,  $\text{ipd\_frac\_multi\_peak} > 2$ , and  $\text{ipd\_gof\_harmonic\_amplitude} \geq 0.1$ .  $\text{ipd\_frac\_multi\_peak}$  corresponds to the fraction of observations for which the source was identified as having two resolved peaks in the image, and therefore is indicative of resolved binaries;  $\text{ipd\_gof\_harmonic\_amplitude}$  indicates the level of variation in the image goodness-of-fit as a function of scan direction, which, if large, would imply the image is asymmetric and therefore suggestive of an unresolved binary;  $\text{ruwe}$  indicates that the astrometric solution does not completely describe the motion of the source, and so can therefore identify unresolved binaries with variable photo-centers (Lindegren et al. 2020b).

I further restricted the sample to those with  $G < 13$ , which are observed within window classes WC0a and WC0b (Lindegren et al. 2020b). These magnitude-defined windows define what pixel mask the source is read out with, and WC0 was divided into two for EDR3: sources with  $11 \lesssim G \lesssim 13$  are observed with the WC0b window and those with  $G \lesssim 11$  with the WC0a window. Magnitude-dependent systematics in the astrometry may therefore be related to the different behavior of photometry in the different window classes (see, e.g., Figure A.4 in Lindegren et al. 2020b). The  $G < 13$  regime is further complicated, however, by the use of differing integration times through the use of “gates,” and which themselves depend on magnitude. I will investigate the possibility of magnitude-dependent errors in corrected Gaia parallaxes in what follows.

I adopt  $\text{nu\_eff\_used\_in\_astrometry}$  (denoted  $\nu_{\text{eff}}$  here) as a proxy for color, following Lindegren et al. (2020a),

<sup>2</sup> Gaia astrometry falls into three classes: stars with position information only (two-parameter solutions); stars with color information from DR2 with enough quality to correct for chromaticity effects (five-parameter solutions); and stars where the color is an additional free parameter in the astrometric solution (six-parameter solutions). The latter two solutions have distinct parallax zero-point properties (Lindegren et al. 2020a, 2020b).

and which is defined based on DR2 photometry for the five-parameter astrometry I use in this analysis (Lindgren et al. 2020b); bluer stars have larger  $\nu_{\text{eff}}$ , and redder stars have smaller  $\nu_{\text{eff}}$ . I did not make cuts in color, because the sample lies well within the regime  $1.24 \mu\text{m}^{-1} < \nu_{\text{eff}} < 1.72 \mu\text{m}^{-1}$ ; outside of this range, the image chromaticity point-spread function and line-spread function corrections are not calibrated, and so there is reason to believe they would suffer from a stronger color-dependent zero-point error (Lindgren et al. 2020a). I will also fit for color-dependent terms to describe residual differences between asteroseismic and Gaia parallaxes in what follows.

The parallax of a star can be derived from the asteroseismic radius via the Stefan–Boltzmann law, written in the following form:

$$\varpi_{\text{seis}}(T_{\text{eff}}, F, R) = F^{1/2} \sigma_{\text{SB}}^{-1/2} T_{\text{eff}}^{-2} R^{-1} = f_0^{1/2} 10^{-1/5(m+BC_b(T_{\text{eff}})-A_b)} \sigma_{\text{SB}}^{-1/2} T_{\text{eff}}^{-2} R^{-1}, \quad (1)$$

where  $R$  is the asteroseismic radius (see below),  $T_{\text{eff}}$  is the effective temperature,  $\sigma_{\text{SB}}$  is the Stefan–Boltzmann constant, and  $F$  is the stellar bolometric flux. Here, I have rewritten the flux in terms of a bolometric correction in the photometric band  $b$ ,  $BC_b$ ; the extinction in that passband,  $A_b$ ; and a magnitude-flux conversion factor that assumes the solar irradiance of  $f_0 = 1.361 \times 10^6 \text{ erg s}^{-1} \text{ cm}^{-2}$  (Mamajek et al. 2015), and an apparent solar bolometric magnitude of  $m_{\text{bol}} = -26.82$  (Torres 2010). I work here with 2MASS  $K_s$  photometry (Skrutskie et al. 2006) to reduce extinction effects. I use a bolometric correction based on MIST models (Paxton et al. 2011, 2013, 2015, 2018, 2019) as implemented in `isoclassify` (Huber et al. 2017; Berger et al. 2020). Visual extinctions were adopted from Rodrigues et al. (2014) and converted into  $A_{K_s}$  assuming  $A_{K_s} = 0.113 A_V$  (Schlafly & Finkbeiner 2011).

The asteroseismic radii required to yield parallaxes according to Equation (1) can be computed according to a scaling relation,

$$\frac{R}{R_{\odot}} \approx \left( \frac{\nu_{\text{max}}}{\nu_{\text{max},\odot}} \right) \left( \frac{\Delta\nu}{f_{\Delta\nu} \Delta\nu_{\odot}} \right)^{-2} \left( \frac{T_{\text{eff}}}{T_{\text{eff},\odot}} \right)^{1/2}, \quad (2)$$

where  $\nu_{\text{max}}$  is an asteroseismic observable that corresponds to the frequency at which stochastically excited oscillations in the stellar envelopes have their highest amplitude and  $\Delta\nu$  is an asteroseismic observable that describes the approximately constant separation in frequency between two oscillation modes of adjacent radial order but the same spherical degree. The former is theoretically and empirically related to stellar surface gravity (Brown et al. 1991; Kjeldsen & Bedding 1995; Chaplin et al. 2008; Belkacem et al. 2011). The latter is related to the mean stellar density (Ulrich 1986; Kjeldsen & Bedding 1995), though there is evidence that the observed  $\Delta\nu$  requires a correction (e.g., White et al. 2011; Guggenberger et al. 2016; Sharma et al. 2016), which is represented in the above by  $f_{\Delta\nu}$ .  $\Delta\nu_{\odot}$  and  $\nu_{\text{max},\odot}$  represent measurements of these quantities for the Sun, to which the scaling relations are tied. The solar reference values of  $\Delta\nu_{\odot} = 135.146 \mu\text{Hz}$  and  $\nu_{\text{max},\odot} = 3076 \mu\text{Hz}$  that I adopt from Pinsonneault et al. (2018) are calibrated such that asteroseismic masses agree with dynamical masses from eclipsing binaries in NGC 6791

(Grundahl et al. 2008; Brogaard et al. 2011, 2012) and NGC 6819 (Jeffries et al. 2013; Sandquist et al. 2013; Brewer et al. 2016).  $f_{\Delta\nu}$ , also adopted from Pinsonneault et al. (2018), amounts to  $\approx 3\%$  corrections of  $\Delta\nu$ , and which vary on a star-by-star basis according to mass, surface gravity, temperature, and metallicity.

In this work, I also consider effectively correcting both  $\Delta\nu$  and  $\nu_{\text{max}}$  using nonlinear scaling relations from Kallinger et al. (2018), which are derived from fits to dynamical surface gravities and mean stellar densities in addition to the open clusters NGC 6791 and NGC 6819:

$$\frac{R}{R_{\odot}} \approx \left( \frac{\nu_{\text{max}}}{\nu_{\text{max,ref}}} \right)^{\kappa} \left( \frac{\Delta\nu}{\Delta\nu_{\text{ref}}} \right)^{-2} \times \left[ 1.0 - \gamma \left( \log_{10} \frac{\Delta\nu}{\Delta\nu_{\text{ref}}} \right)^2 \right]^2 \left( \frac{T_{\text{eff}}}{T_{\text{eff},\odot}} \right)^{1/2}, \quad (3)$$

where  $\kappa = 1.0075 \pm 0.0021$ ,  $\gamma = 0.0043 \pm 0.0025$ , and I use the  $\Delta\nu_{\text{ref}}$  value from Kallinger et al. (2018) appropriate for the method of deriving APOKASC-2  $\Delta\nu$  values,  $\Delta\nu_{\text{ref}} = 133.1 \pm 1.3 \mu\text{Hz}$ . I adopt  $\nu_{\text{max,ref}} = 3076 \mu\text{Hz}$  (Pinsonneault et al. 2018). In what follows, I marginalize over errors in the asteroseismic radii due to, e.g., the choice of  $\nu_{\text{max,ref}}$  or  $\Delta\nu$  corrections, by fitting for a multiplicative factor that brings the radii into agreement with the Gaia parallaxes.

I conservatively restricted the analysis to stars with  $R < 30 R_{\odot}$ , based on findings from Zinn et al. (2019b) that asteroseismic radii are likely inflated in the evolved red giant regime. I also restricted the analysis to the first-ascent red giant branch stars with  $15 \mu\text{Hz} < \nu_{\text{max}} < 200 \mu\text{Hz}$  and  $2 \mu\text{Hz} < \Delta\nu < 10 \mu\text{Hz}$ , which is the range occupied by the majority of the open cluster calibrators used by Pinsonneault et al. (2018) and Kallinger et al. (2018) to set the  $\nu_{\text{max}}/\Delta\nu$  solar reference values/corrections. For parts of the following analysis using the Yu et al. (2018) data set, I use the nonlinear scaling relations of Equation (3), because the APOKASC-2  $\Delta\nu$  corrections ( $f_{\Delta\nu}$  in Equation (2)) assume the  $\nu_{\text{max}}$  and  $\Delta\nu$  of the APOKASC-2 catalog.

### 3. Methods

The approach I take to investigate the need, if any, for adjustments to the  $Z_5$  five-parameter solution parallax zero-point model is to compare Gaia parallaxes corrected using  $Z_5$  to asteroseismic parallaxes. By taking the difference between the corrected Gaia parallaxes and the asteroseismic parallaxes, which I refer to as the parallax residuals in what follows, one can simultaneously constrain asteroseismic parallax problems due to asteroseismic radius and any additive problems in the Gaia parallax that may remain after correction according to  $Z_5$ . The simultaneous calibration is possible because errors in the asteroseismic parallax due to the asteroseismic radius will be fractional and therefore dependent on parallax, given the multiplicative dependence of asteroseismic parallax on the asteroseismic radius (Equation (1)). By contrast, Gaia parallax zero-point problems are found to be additive and can be described by terms that depend on magnitude, position, and color (Lindgren et al. 2020a).

Formally speaking, the model for describing any adjustments to the  $Z_5$  model can therefore be described as a likelihood of the



form

$$\begin{aligned} & \mathcal{L}(c, d, e, a, k, g, s | \hat{\varpi}_{\text{Gaia}}, T_{\text{eff}}, \Delta\nu, \nu_{\text{max}}, A_{K_s}, \\ & K_s, BC, \nu_{\text{eff}}, G, \sin \beta) \\ & \propto \frac{1}{\sqrt{(2\pi)^N |C'|}} \exp \left[ -\frac{1}{2} (\mathbf{y} - \mathbf{x})^T C'^{-1} (\mathbf{y} - \mathbf{x}) \right]. \end{aligned} \quad (4)$$

In the above,

$$\mathbf{y} \equiv Y(a, d_a, \nu_{\text{eff}}) \varpi_{\text{seis}}(T_{\text{eff}}, \Delta\nu, \nu_{\text{max}}, A_{K_s}, K_s, BC)$$

and

$$\mathbf{x} \equiv \hat{\varpi}_{\text{Gaia}} - Z_5(\nu_{\text{eff}}, G, \sin \beta) + \Delta Z(c, d, e, \nu_{\text{eff}}, G),$$

where

$$Y(a, d_a, \nu_{\text{eff}}) \equiv 1 - a + d_a(\nu_{\text{eff}} - 1.48) \quad (5)$$

describes fractional errors in asteroseismic parallaxes:  $a$  describes errors in the asteroseismic radius scale due to, e.g., solar reference value choice, and would be unity in the absence of any. As I discuss in Section 4.1, the term  $d_a$  describes color-dependent corrections to the asteroseismic parallaxes due to, e.g., bolometric correction systematics that are a function of temperature/color.

$\Delta Z$  is the model for the residual parallax difference left unexplained by the  $Z_5$  model.  $\hat{\varpi}_{\text{Gaia}}$  is the raw EDR3 parallax,  $\sin \beta$  is the sine of ecliptic latitude, and  $Z_5$  is evaluated using the Python implementation of the correction, `zero_point`.<sup>3</sup> I will only be using Gaia parallaxes corrected in this way in the analysis, which I denote  $\varpi_{\text{Gaia}}$ , as opposed to the raw Gaia parallaxes, denoted  $\hat{\varpi}_{\text{Gaia}}$ .

I consider several different forms for  $\Delta Z$ , allowing for a local offset to the corrected Gaia parallaxes as well as color- and magnitude-dependent terms. Because I only analyze stars in the Kepler field, it is not possible to constrain ecliptic latitude-dependent terms as the Gaia team has done for the  $Z_5$  model (though it is possible to statistically infer the level of small-scale variations as a function of angular scale, as I discuss below and in Section 4.7). At its most complicated, the model for the parallax residuals takes the form

$$\Delta Z(c, d, e, \nu_{\text{eff}}, G) = \begin{cases} c + c_2 + d_1(\nu_{\text{eff}} - 1.48) \\ + d_3(1.48 - \nu_{\text{eff}})^3 + e_1(G - 12.2) \\ - \Delta Z_{G=13}, \\ \text{for } G < 10.8 \\ c + d_2(\nu_{\text{eff}} - 1.48) \\ + d_3(1.48 - \nu_{\text{eff}})^3 + e_2(G - 12.2) \\ - \Delta Z_{G=13}, \\ \text{for } G \geq 10.8. \end{cases} \quad (6)$$

I consider nested models under various permutations of the parameters,  $c, d, e$ , etc., as listed in Table 1; a blank entry indicates an unused parameter, such that it can be considered to be zero in Equation (6). In some models, there is a single color term across all magnitudes, i.e.,  $d_1 \equiv d_2 \equiv d$ . Models otherwise differ by removing any number of terms by setting them to zero (e.g., the preferred model, Model 0, has a single color term and no magnitude term, i.e.,  $d_1 \equiv d_2 \equiv d$  and  $e_1 \equiv e_2 \equiv e = 0$ ). The term  $\Delta Z_{G=13}$  is not a fitted parameter, but rather a constant

defined such that  $c$  describes the mean offset at  $G = 13$  and  $\nu_{\text{eff}} = 1.48 \mu\text{m}^{-1}$  remaining after correction with  $d$  and/or  $d_3$ , viz.,  $\Delta Z_{G=13} \equiv 0.8e_2 \mu\text{as}$ .  $c$  therefore can be interpreted as the average local offset of EDR3 parallaxes with respect to the rest of the sky/quasar frame of reference that the  $Z_5$  model was calibrated to. The pivot point of  $\nu_{\text{eff}} = 1.48 \mu\text{m}^{-1}$  is chosen to be consistent with the  $q_{1k}$  and  $q_{2k}$  color terms in the  $Z_5$  model, which take the form  $(\nu_{\text{eff}} - 1.48)$  and  $(1.48 - \nu_{\text{eff}})^3$  (Lindgren et al. 2020a), respectively. The pivot point of  $G = 10.8$  is motivated by the piecewise functions in magnitude used to describe the magnitude dependence of  $Z_5$  and which have a breakpoint at 10.8. This is also in the transition region of  $G \approx 11$  between the window classes WC0a and WC0b. The faintest breakpoint in the  $Z_5$  model that overlaps with the sample's magnitude range occurs at  $G = 12.2$ , which sets the pivot point for the  $e$  term.

Note that one is able to simultaneously constrain (1) fractional errors in the asteroseismic radii, which would naturally arise from problems in the radius-scaling relation (Equation (3)) entering into the asteroseismic parallaxes (Equation (1)) as parameterized by the  $a$  and  $d_a$  terms in Equation (5), as well as (2) additive errors in the corrected Gaia parallaxes, as parameterized by the  $c, d$ , and  $e$  terms in Equation (6).

The elements of the covariance matrix in Equation (4) are given by

$$\begin{aligned} C'_{ij} = & C_{ij} + k^2 \delta_{ij} \sigma_{\varpi_{\text{Gaia}}}^2 + \left[ g^2 + \left( \frac{\partial Y}{\partial \varpi_{\text{seis}}} \right)^2 \right] \delta_{ij} \sigma_{\varpi_{\text{seis}}}^2 \\ & + \left[ \left( \frac{\partial Y}{\partial \nu_{\text{eff}}} \right)^2 + \left( \frac{\partial \Delta Z}{\partial \nu_{\text{eff}}} \right)^2 \right] \delta_{ij} \sigma_{\nu_{\text{eff}}}^2 + \left( \frac{\partial \Delta Z}{\partial G} \right)^2 \delta_{ij} \sigma_G^2 \\ & + \delta_{ij} s^2, \end{aligned} \quad (7)$$

and describe the covariance between the asteroseismic–Gaia parallax difference for two stars,  $i$  and  $j$ , where  $\delta_{ij}$  is the Kronecker delta function. In the above,  $k$  and  $g$  describe corrections to the formal statistical uncertainties of Gaia and asteroseismic parallaxes, which can be constrained because the two uncertainties are not strongly correlated (see Section 4.6).  $s$  can be thought of as an intrinsic scatter in the parallax residuals that capture any variation not described by the model, or, alternatively, as an additive correction to the Gaia and/or asteroseismic parallax uncertainties.  $\sigma_G$  is the uncertainty on  $G$ , and  $\sigma_{\nu_{\text{eff}}}$ , the uncertainty in `nu_eff_used_in_astrometry`, is adopted to be 1% of  $\nu_{\text{eff}}$ , because the latter is a fixed and not fitted quantity for five-parameter astrometric solutions—this is  $\approx 2$  times larger than the uncertainty in `astrometric_pseudo_colour`, which is a fitted color as part of the six-parameter solutions. The statistical uncertainties in the asteroseismic parallaxes are denoted  $\sigma_{\varpi_{\text{seis}}}$  and include contributions from  $\Delta\nu, \nu_{\text{max}}, T_{\text{eff}}, A_{K_s}, K_s$ , and  $BC$  via linear propagation of uncertainty. The Gaia spatially correlated errors are encapsulated in  $C_{ij}$ , which describes the spatial covariance in Gaia parallax between stars  $i$  and  $j$  separated by an angular distance,  $\theta_{ij}$ .

By appealing to quasars in EDR3, Lindgren et al. (2020b) fit an exponential function to the parallax spatial covariance for  $\theta_{ij} \gtrsim 0.5^\circ$  of  $C_{ij, \text{QSO}} = \rho_{\text{QSO}} e^{(-\ln 2 \theta_{ij} / \theta_{1/2, \text{QSO}})}$ , with  $\rho_{\text{QSO}} = 142 \mu\text{as}^2$  and  $\theta_{1/2, \text{QSO}} \approx 11^\circ$ .

<sup>3</sup> [https://gitlab.com/icc-ub/public/gaiadr3\\_zero\\_point/-/tree/master](https://gitlab.com/icc-ub/public/gaiadr3_zero_point/-/tree/master)

**Table 1**  
Best-fitting Gaia EDR3 Parallax Zero-point Model Adjustment Parameters

Model (#)	$\Delta\text{BIC}^a$	$c$ ( $\mu\text{as}$ )	$c_2$ ( $\mu\text{as}$ )	$d$ ( $\mu\text{as } \mu\text{m}$ )	$d_1$ ( $\mu\text{as } \mu\text{m}$ )	$d_2$ ( $\mu\text{as } \mu\text{m}$ )	$d_3$ ( $\mu\text{as } \mu\text{m}^3$ )	$d_u$ ( $\mu\text{m}$ )
(0)	0.0	$-14.6 \pm 1.8$	$-15 \pm 3$	$-303 \pm 25$	...	...	...	...
$e$ no $a$ (1)	-4.7	$-13.1 \pm 1.0$	$-17 \pm 3$	$-289 \pm 24$	...	...	...	...
$d_u$ (2)	1.1	$-12.9 \pm 1.9$	$-15 \pm 3$	$-222 \pm 40$	...	...	...	$-0.14 \pm 0.06$
$e$ (3)	2.8	$-13.6 \pm 1.8$	$-17 \pm 3$	$-292 \pm 26$	...	...	...	...
$d_1 d_2$ (4)	6.7	$-14.6 \pm 1.8$	$-19 \pm 5$	...	$-437 \pm 134$	$-298 \pm 26$	...	...
$d_3$ (5)	6.9	$-14.2 \pm 1.8$	$-15 \pm 3$	$-280 \pm 34$	...	...	$6710 \pm 7518$	...
$s$ (6)	7.7	$-14.5 \pm 1.8$	$-15 \pm 3$	$-301 \pm 25$	...	...	...	...
$e_1 e_2$ (7)	10.4	$-13.6 \pm 1.9$	$-20 \pm 13$	$-292 \pm 25$	...	...	...	...
no $c_2$ (8)	14.9	$-11.5 \pm 1.7$	...	$-293 \pm 25$	...	...	...	...
$d_u$ no $d$ (9)	22.1	$-6.1 \pm 1.5$	$-14 \pm 3$	...	...	...	...	$-0.37 \pm 0.03$
no $c$ (10)	58.8	...	$-6 \pm 3$	$-180 \pm 20$	...	...	...	...
no $d$ (11)	137.8	$-1.2 \pm 1.4$	$-12 \pm 3$	...	...	...	...	...
$k$ $g$ (12)	-105.4	$-14.4 \pm 1.6$	$-14 \pm 2$	$-340 \pm 24$	...	...	...	...
El-BadryRixHeintz2021 $k$ $g$ (13)	... <sup>b</sup>	$-15.6 \pm 1.7$	$-14 \pm 2$	$-353 \pm 24$	...	...	...	...
Yu+2018 (14)	... <sup>b</sup>	$-14.5 \pm 1.8$	$-17 \pm 3$	$-182 \pm 27$	...	...	...	...
$e$ Yu+2018 (15)	7.6 <sup>b</sup>	$-14.4 \pm 1.8$	$-17 \pm 3$	$-181 \pm 27$	...	...	...	...
Kallinger+2018 (16)	... <sup>b</sup>	$-15.4 \pm 1.8$	$-14 \pm 3$	$-212 \pm 25$	...	...	...	...
$e$ Kallinger+2018 (17)	0.6 <sup>b</sup>	$-14.3 \pm 1.8$	$-17 \pm 3$	$-201 \pm 25$	...	...	...	...
$e$ ( $\mu\text{as mag}^{-1}$ )	$e_1$ ( $\mu\text{as mag}^{-1}$ )	$e_2$ ( $\mu\text{as mag}^{-1}$ )	$a$	$k$	$g$	$s$ ( $\mu\text{as}$ )	$\chi^2/\text{dof}^c$	$N$
...	...	...	$0.995 \pm 0.002$	...	...	...	0.760*****	2130
...	$-2.6 \pm 0.9$	...	...	...	...	...	0.755*****	2130
...	...	...	$0.998 \pm 0.002$	...	...	...	0.769*****	2130
$-2.4 \pm 1.1$	...	...	$0.999 \pm 0.003$	...	...	...	0.756*****	2130
...	...	...	$0.995 \pm 0.002$	...	...	...	0.760*****	2130
...	...	...	$0.996 \pm 0.002$	...	...	...	0.766*****	2130
...	...	...	$0.996 \pm 0.002$	...	...	$0 \pm 1$	0.761*****	2130
...	$-4.0 \pm 7.1$	$-2.4 \pm 1.1$	$0.999 \pm 0.003$	...	...	...	0.756*****	2130
...	...	...	$1.000 \pm 0.002$	...	...	...	0.766*****	2130
...	...	...	$1.005 \pm 0.002$	...	...	...	0.767*****	2130
...	...	...	$1.011 \pm 0.001$	...	...	...	0.797*****	2130
...	...	...	$1.002 \pm 0.002$	...	...	...	0.863****	2130
...	...	...	$0.997 \pm 0.002$	$1.22 \pm 0.06$	$0.69 \pm 0.03$	...	0.999	2130
...	...	...	$0.996 \pm 0.002$	$1.02 \pm 0.04$	$0.70 \pm 0.03$	...	0.998	2151
...	...	...	$0.984 \pm 0.002$	...	...	...	0.904***	2114
$0.0 \pm 1.1$	...	...	$0.984 \pm 0.003$	...	...	...	0.904***	2114
...	...	...	$0.978 \pm 0.002$	...	...	...	0.805*****	2140
$-2.9 \pm 1.1$	...	...	$0.983 \pm 0.003$	...	...	...	0.798*****	2140

**Notes.** Best-fitting parameters for models based on Equation (4), according to MCMC analysis using the likelihood of Equation (4).  $N$  denotes the number of stars in the sample used for the fit.

<sup>a</sup> The difference in the Bayesian Information Criterion between a given model and Model 0, where a smaller  $\Delta\text{BIC}$  indicates a more preferred model.

<sup>b</sup> Models 13–17 use data incommensurate with the data used for Models 0–12, so Model 13 has  $\Delta\text{BIC}$  set to 0; Models 14–15 have  $\Delta\text{BIC}$  listed with respect to Model 14; and Models 16–17 with respect to Model 16.

<sup>c</sup> Asterisks indicate the significance of the deviation of  $\chi^2/\text{dof}$  from unity, with one asterisk for each  $\sigma$ , capped at  $5\sigma$ .

**Table 2**  
Gaia EDR3 Parallax Spatially Correlated Systematic Uncertainties

$\rho$	$\theta_{1/2}$	$\chi^2/\text{dof}$	$N$	
$15_{-9}^{+9} \mu\text{as}^2$	$0.49_{-0.17}^{+0.17}\text{deg}$	2.9	37	
$\sqrt{C_{ij}(\theta_{ij} = \theta_{1/2})^{\text{a}}}$	$\sqrt{C_{ij}(\theta_{ij} = 0^\circ)^{\text{a}}}$	$\sqrt{C_{ij}(\theta_{ij} = 0^\circ 5')^{\text{a}}}$	$\sqrt{C_{ij}(\theta_{ij} = 1^\circ)^{\text{a}}}$	$\sqrt{C_{ij}(\theta_{ij} = 5^\circ)^{\text{a}}}$
$2.5_{-0.8}^{+0.6} \mu\text{as}$	$3.9_{-1.4}^{+1.1} \mu\text{as}$	$2.5_{-0.8}^{+0.6} \mu\text{as}$	$1.6_{-0.6}^{+0.5} \mu\text{as}$	$0.1_{-0.1}^{+0.1} \mu\text{as}$

**Notes.** Best-fitting parameters for spatially correlated uncertainties of Gaia parallaxes, as inferred in the Kepler field and parameterized by Equation (8).  $\rho$  describes the variance at small scales.  $\theta_{1/2}$  is the characteristic angular scale for the spatially correlated uncertainties.

<sup>a</sup> The square root of the covariance,  $C$ , is a measure of the systematic uncertainty in the Gaia parallaxes due to spatial correlations.

In this work, I derive an estimate of the spatial covariance matrix (Section 4.7), modeling it with an equation of the same form as  $C_{ij,\text{QSO}}$ :

$$C_{ij} = \begin{cases} \rho e^{(-\ln 2 \theta_{ij} / \theta_{1/2})}, & \text{for } 0^\circ < \theta_{ij} \leq 10^\circ \\ 0, & \text{otherwise,} \end{cases} \quad (8)$$

with best-fitting parameters according to Table 2. Note that  $\theta_{1/2}$  is defined analogously to the half-angle in the Gaia team description of the covariance,  $\theta_{1/2,\text{QSO}}$ . I tested the impact of spatial covariance in the likelihood analysis using an approximation described in Zinn et al. (2017). Briefly, I divided the Kepler field into  $\sim 2.5 \times 2.5$  squares corresponding to the Kepler modules, treating each one as independent from the other, given that spatially correlated Gaia parallax errors are  $\approx 1\%$  the level of statistical uncertainties on scales larger than  $3^\circ$  (see Section 4.7). The results thus accounting for spatial correlations are not significantly different from those without spatial correlations, and so I ignore the spatial covariance term in Equation (7),  $C_{ij}$ , in what follows. I describe how I infer the spatial covariance in Gaia parallaxes and present the fit to Equation (8) in Section 4.7.

#### 4. Results and Discussion

I fit the model of Equation (4) using Markov Chain Monte Carlo (MCMC), rejecting from analysis stars whose Gaia and asteroseismic parallaxes disagree by more than  $2.5\sigma$ . Figure 1 shows the resulting posterior distributions of the parameters for the preferred model (Model 0 in Table 1). The best-fitting parameters are provided in Table 1, which are taken to be the means of the posteriors; the uncertainties are taken to be the standard deviations of the posteriors. I also provide the Bayesian Information Criterion difference ( $\Delta\text{BIC}$ ; Schwarz 1978) for all models that I considered compared to the preferred model, where a smaller value indicates stronger evidence for the model, and a difference in 6 between models is taken to be a strong preference (Kass & Raftery 1995). In what follows, I take a conservative approach to potential adjustments to  $Z_5$ , by default assuming terms in  $\Delta Z$  are null unless there is strong evidence for them.

Before correction by  $Z_5$ , the raw Gaia and asteroseismic parallaxes have a mean difference of  $+22 \mu\text{as}$  (scatter of  $23 \mu\text{as}$ ), in the sense that Gaia parallaxes are smaller than asteroseismic parallaxes. Even before correction according to  $Z_5$ , this is a significant improvement over the  $\approx +50 \mu\text{as}$  underestimation of DR2 parallaxes compared to asteroseismic parallaxes for this sample of red giant branch stars (Zinn et al. 2019a). For stars with  $G > 10.8$ , correcting the Gaia parallaxes

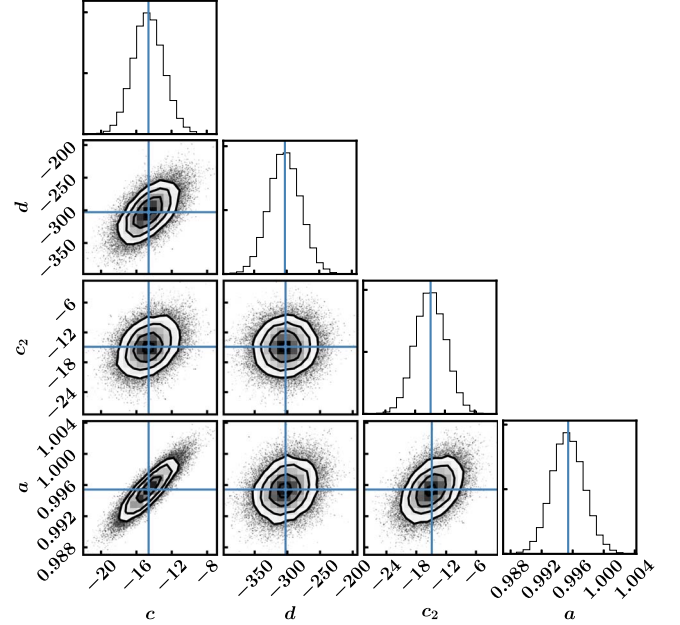


**Figure 1.** Posterior distributions of the parameters describing residual corrections to the  $Z_5$  model required to bring corrected Gaia parallaxes into agreement with asteroseismic parallaxes, according to Equations (5) and (6). Best-fitting parameter values are provided in Table 1 (Model 0).

according to  $Z_5$ , adjusting the asteroseismic radii with  $a$ , and removing the local offset unique to the Kepler field  $c$ , yields a residual of  $+9 \mu\text{as}$ , which is due to a color trend. I note that a nonzero color term,  $d$ , is strongly preferred to fit the parallax residuals. However, I take caution in interpreting this term as solely due to adjustments needed of  $Z_5$ . As I explain in Section 4.1, the color term as fitted in Model 0,  $d$ , may have contributions due to color-dependent asteroseismic parallax errors ( $d_a$  in Equation (5)), for which there is not strong enough evidence to confirm. Under a conservative assumption, removing finally the color term implies the  $Z_5$  model leaves an insignificant residual of  $+0.3 \mu\text{as}$ , with uncertainty in the mean of this residual of  $0.4 \mu\text{as}$ . For stars with  $G \lesssim 11$ , the  $Z_5$  model appears to overcorrect the parallaxes by  $-15 \pm 3 \mu\text{as}$ , as I discuss in Section 4.4.

The parallax residuals (asteroseismic –  $Z_5$ -corrected Gaia) modeled here are shown as a function of asteroseismic parallax and various other parameters in Figures 2 and 3. The observed difference between corrected Gaia parallaxes and asteroseismic parallaxes is shown as error bars, and the best-fitting, preferred model to describe these residuals,  $\Delta Z$  (Equation (6) and

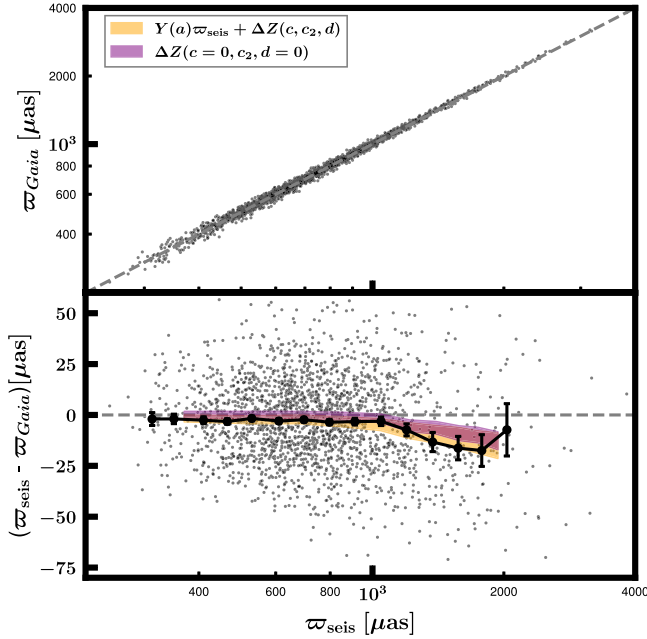


**Figure 2.** Residuals of the difference between the asteroseismic and Gaia parallax corrected according to the Lindegren et al. (2020a)  $Z_5$  model as a function of asteroseismic parallax,  $\varpi_{\text{seis}}$ . The black error bars show the binned weighted means of the parallax residuals. The yellow band represents a running weighted mean of the best-fitting model (Model 0 in Table 1) described by Equations (5) and (6), and which includes an additive offset, a rescaling of the asteroseismic parallax, and a color-dependent term (the width of the band encompasses a  $\pm 1\sigma$  region in the offsets,  $c$  and  $c_2$ , and  $\pm 0.5\sigma$  in the color term,  $d$ ). The purple band shows a model without accounting for errors in the asteroseismic radii ( $Y(a, d_a) = 0$ ; see Equation (5) and Sections 4.1 and 4.2) or a local offset in Gaia parallaxes unique to the region of the sky analyzed here ( $c = 0$ ; see Equation (6) and Section 4.3).

parameters from Model 0 in Table 1), is shown as the yellow band. The purple band shows the model for what the parallax residuals would look like if the asteroseismic radii were exactly on the Gaia parallactic scale (i.e.,  $Y(a) = 0$ ), assuming there is no color term in  $\Delta Z$  ( $e = 0$ ) or in asteroseismic parallax ( $d_a = 0$ ), and in the absence of a local offset for the Kepler field’s part of the sky ( $c = 0$ ). As such, it represents the  $c_2$  term of Equation (6), and which is the adjustment to the  $Z_5$  model for which there is the strongest evidence (Section 4.4). The purple band thus demonstrates that the  $Z_5$  model performs very well for  $G \gtrsim 11$ , apart from a constant, local offset for the Kepler field not shown by the purple band ( $c = -15 \pm 2 \mu\text{as}$  from Model 0 in Table 1).

Below, I discuss aspects of the parallax residuals as a function of the different terms in Equation (6), considering evidence for not only refinements to the  $Z_5$  model with a Kepler field-specific local offset,  $c$ ; a color term,  $d$ ; and a magnitude term,  $e$ ; but also evidence for corrections to the asteroseismic parallaxes with the color term,  $d_a$ , and the asteroseismic radius-rescaling term,  $a$ . I also discuss the uncertainty budget in the parallax difference, including evidence for corrections to the fractional parallax uncertainties and quantifying systematic spatial variations in Gaia parallaxes.

#### 4.1. Corrections to Gaia and Asteroseismic Parallaxes: The Color Term

It should first be noted that the color term in this analysis,  $d$ , describes a smaller range in  $\nu_{\text{eff}}$  ( $1.4 \mu\text{m}^{-1} \lesssim \nu_{\text{eff}} \lesssim 1.5 \mu\text{m}^{-1}$ )

than the linear color terms  $q_{1k}$  of the  $Z_5$  model attempt to explain ( $1.24 \mu\text{m}^{-1} \lesssim \nu_{\text{eff}} \lesssim 1.72 \mu\text{m}^{-1}$ ). This means that stronger local gradients in the parallax systematics may still remain after correction by  $Z_5$ , which the sample could be sensitive to. The sample will be most sensitive to color trends between  $12 \lesssim G \lesssim 13$ , where most of the data are, meaning that any color-dependent refinement to  $Z_5$  I find are not necessarily valid in other magnitude regimes and may not describe color trends within the brighter range of the sample,  $9 \lesssim G \lesssim 12$ .

With these caveats in mind, a significant color term of  $d = -300 \pm 25 \mu\text{as} \mu\text{m}$  is strongly favored to describe the parallax residuals (Model 11 versus Model 0). This trend is also clearly visible in Figure 4(e).

Here, I take care to consider the possibility that  $d$  may not only describe an additive correction to EDR3 parallaxes but also may partially describe small problems in the asteroseismic parallax via the bolometric correction and/or  $\Delta\nu$  correction.

Regarding possible contributions to  $d$  from the asteroseismic parallaxes, consider, for example, that bolometric corrections used to calculate the asteroseismic parallax (Equation (1)) are found to vary as a function of temperature/color depending on the prescription by  $\approx 2\%$ – $4\%$  (Zinn et al. 2019b; Tayar et al. 2020). This is enough to explain some of the color dependence of the parallax difference: for a median parallax of the sample of  $\approx 0.7 \text{ mas}$ , the resulting effect on the asteroseismic parallaxes would be  $7\text{--}14 \mu\text{as}$ , corresponding to differences in  $\approx 70\text{--}100 \mu\text{as} \mu\text{m}$  in  $d$ , which is comparable to the best-fitting color term of  $d_2 = -300 \pm 25 \mu\text{as} \mu\text{m}$ .

Additional color residuals may come about through the choice of the  $\Delta\nu$  correction, which depends on temperature and therefore color. I test the sensitivity of the color trend to  $\Delta\nu$  corrections by considering the nonlinear scaling relations of Kallinger et al. (2018) instead of the APOKASC-2  $\Delta\nu$  corrections (Model 16). The resulting color term of  $-210 \pm 25 \mu\text{as} \mu\text{m}$  reveals a  $\approx 100 \mu\text{as} \mu\text{m}$  level variation due to the  $\Delta\nu$  correction choice. Similarly, the Yu et al. (2018) data using the same nonlinear scaling relations yield  $d = -180 \pm 30 \mu\text{as} \mu\text{m}$  (Model 14). Taken together, these differences of  $\sim 100 \mu\text{as} \mu\text{m}$  are suggestive of the level of color-dependent uncertainties in  $\Delta\nu$  corrections used to calibrate asteroseismic radii.

Due to these indications of contributions to  $d$  from asteroseismic parallax systematics instead of EDR3 parallax systematics, I considered a color-dependent correction explicitly for the asteroseismic parallaxes of the form  $d_a \varpi_{\text{seis}} (\nu_{\text{eff}} - 1.48)$  (Equation (5)). This term is designed to capture color systematics in the asteroseismic parallax, which will tend to be fractional (dependent on  $\varpi_{\text{seis}}$ ), given that bolometric corrections and  $\Delta\nu$  enter multiplicatively in Equation (1). (The same rationale motivates the fractional correction to asteroseismic parallaxes,  $a$ , in Equation (5).) Simultaneously allowing for an additive color term,  $d$ , and this fractional term,  $d_a$ , yields  $d_a = -0.14 \pm 0.06 \mu\text{m}$  and a less substantial  $d = -220 \pm 40 \mu\text{as} \mu\text{m}$  (Model 2). For the typical star in the sample with  $\varpi_{\text{seis}} \approx 700 \mu\text{as}$ , this value of  $d_a$  corresponds to a color term due to systematics in the asteroseismic parallax of  $\approx -100 \mu\text{as} \mu\text{m}$ , which is consistent with expectations as outlined above. Nevertheless, there is no strong evidence (i.e.,  $\Delta\text{BIC} < -6$ ) for adding  $d_a$  either as a replacement for the additive color correction (Model 9 versus Model 0) or in addition to  $d$  (Model 2 versus Model 0). I therefore conservatively correct for a color term in what follows, without definitely attributing it fully to Gaia parallax systematics. To be sure, a color correction of some sort is required to explain the parallax residuals, though it is likely



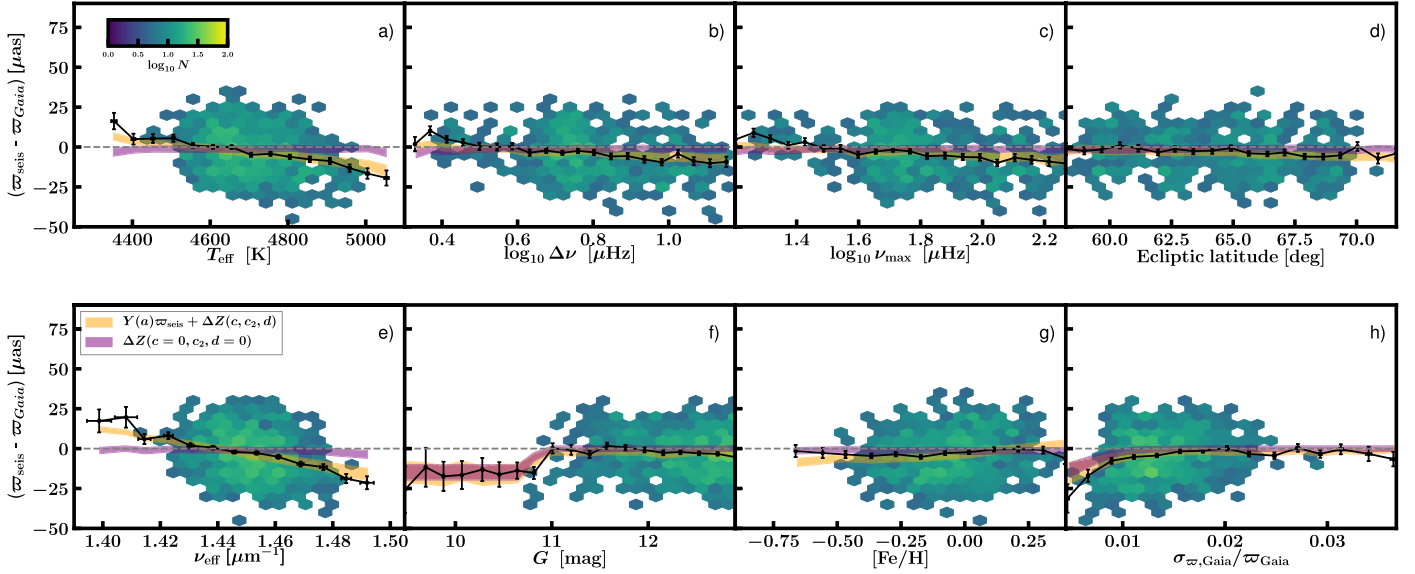


**Figure 3.** Residuals of the difference between the asteroseismic and Gaia parallax corrected according to the Lindegren et al. (2020a)  $Z_5$  model as a function of  $T_{\text{eff}}$  (a),  $\Delta\nu$  (b),  $\nu_{\text{max}}$  (c), ecliptic latitude (d),  $\nu_{\text{eff}}$  (e),  $G$  (f),  $[\text{Fe}/\text{H}]$  (g), and fractional Gaia parallax uncertainty,  $\sigma_{\pi, \text{Gaia}}/\varpi_{\text{Gaia}}$  (h). Black error bars show binned weighted means of the parallax residuals. The yellow band represents a running weighted mean of the best-fitting model (Model 0 in Table 1) described by Equations (5) and (6), and which includes an additive offset, a rescaling of the asteroseismic parallax, and a color-dependent term (the width of the band encompasses a  $\pm 1\sigma$  region in the offsets,  $c$  and  $c_2$ , and  $\pm 0.5\sigma$  in the color term,  $d$ ). The purple band shows a model without accounting for errors in the asteroseismic radii ( $Y(a, d_a) = 0$ ; see Equation (5), and Sections 4.1 and 4.2) or a local offset in Gaia parallaxes unique to the region of the sky analyzed here ( $c = 0$ ; see Equation (6) and Section 4.3), and which has the same meaning as the purple band in Figure 2. The hexagonal bins represent the density of points, as indicated by the color bar in panel (a); for clarity, bins with fewer than five points are not shown.

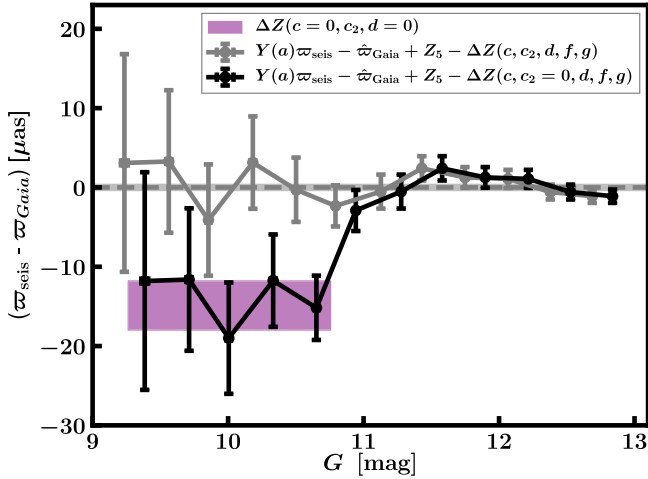


**Figure 4.** Binned, weighted means of the difference between asteroseismic and Gaia parallax corrected according to the Lindegren et al. (2020a)  $Z_5$  model as a function of  $G$  are shown as black error bars, after further corrections with a color term, a constant offset, and a rescaling of the asteroseismic radii (according to Equations (5) and (6) with parameters from Model 0 in Table 1, except with  $c_2 = 0$ ). The purple shaded region represents the additive adjustment,  $c_2$ , to the Gaia team's  $Z_5$  parallax zero-point model required to bring  $Z_5$ -corrected EDR3 parallaxes into alignment with asteroseismic parallaxes (the bandwidth corresponds to the  $1\sigma$  confidence interval for  $c_2$ ); corrected EDR3 parallaxes for  $G < 10.8$  are thus inferred to be  $15 \pm 3 \mu\text{as}$  too large. Other terms in Equation (6) are either not strongly preferred by the data or likely to be specific to the Kepler field (e.g.,  $c$ ). After the adjustment of the  $Z_5$  model according to the purple band, the parallax residuals reduce to the gray error bars, which have been shifted horizontally for clarity. The gray band indicates that the  $Z_5$ -corrected Gaia parallaxes agree with asteroseismic parallaxes for stars in the sample with  $9 \lesssim G \lesssim 13$ ,  $1.4 \mu\text{m}^{-1} \lesssim \nu_{\text{eff}} \lesssim 1.5 \mu\text{m}^{-1}$  to within on average  $\pm 0.4 \mu\text{as}$  after the bright-end adjustment to  $Z_5$  of  $c_2 = -15 \mu\text{as}$ .

partially due to an additive adjustment needed of  $Z_5$  as well as a properly parallax-dependent color term arising from bolometric correction and  $\Delta\nu$  systematics.

Non-Gaia contributions notwithstanding, there would appear to remain a  $\approx -200 \mu\text{as} \mu\text{m}$  residual that would be attributable to color residuals in the  $Z_5$  model. In this regard, one can helpfully refer to the consistency check performed by the Gaia team in the LMC. On average, there is not a large gradient in the LMC parallax across the whole range  $1.1 \mu\text{m}^{-1} \lesssim \nu_{\text{eff}} \lesssim 1.9 \mu\text{m}^{-1}$  after correction by the Gaia zero-point model (Figure 23 of Fabricius et al. 2020). However, it is clear that gradients exist on smaller scales, which, for  $1.4 \mu\text{m}^{-1} \lesssim \nu_{\text{eff}} \lesssim 1.5 \mu\text{m}^{-1}$ , is approximately  $-140 \mu\text{as} \mu\text{m}$ , in the sense that bluer stars have too-small parallaxes. Although most of the LMC members used by the Gaia team have  $G > 13$ , this nonetheless indicates that linear residuals in parallax as a function of color exist after correction by  $Z_5$ . Moreover, this gradient is similar in magnitude but opposite in sign to the gradient I identify. Recalling that the sines of the ecliptic latitudes of the LMC and Kepler field are approximately the same magnitude ( $\approx 1$ ) but of opposite signs, this is suggestive of a refinement to the  $q_{01}$  term for  $G = 12.2$  in the  $Z_5$  model:  $q_{01}$  sets the magnitude of a correction of the form  $\sin \beta(\nu_{\text{eff}} - 1.48)$ , and an increase from  $\approx 40 \mu\text{as} \mu\text{m}$  adopted for the  $Z_5$  model to at least  $100 \mu\text{as} \mu\text{m}$  could seemingly be accommodated, given the uncertainties in  $q_{01}$  (Figure 11 of Lindegren et al. 2020a). Keeping in mind both the potential errors in the  $Z_5$  coefficients due to the bootstrap fitting approach in the bright regime ( $G < 10.8$ ; Lindegren et al. 2020a) and the two times larger range in color explained by the  $q_{01}$  term as opposed to  $d$ , I believe this is a plausible scenario.

I attempted to model the color-dependent residuals with the addition of a cubic term in the color dependence ( $d_3$  in Equation (6)), which was motivated by the Gaia team's cubic term in  $Z_5$ ,  $q_{20}$ . However,  $d_3$  is strongly disfavored compared to having no cubic term, according to the  $\Delta\text{BIC}$  in Table 1 (Model 5 versus Model 0). The data also prefer having a single



color term instead of one to describe  $G < 10.8$  and one to describe  $G \geq 10.8$ , as is seen from the difference in  $\Delta\text{BIC}$  between Model 4 and Model 0.

#### 4.2. Corrections to Asteroseismic Parallaxes: The Radius-rescaling Term

I note that the radius-rescaling term of  $a = 0.995 \pm 0.002$  for the preferred model (Model 0 in Table 1) is consistent within  $2\sigma$  with the value of  $1.015 \pm 0.003$  (stat.)  $\pm 0.013$  (syst.) for stars with  $3.5R_{\odot} \leq R \leq 10R_{\odot}$  as well as the value of  $1.019 \pm 0.006$  (stat.)  $\pm 0.013$  (syst.) for  $10R_{\odot} < R < 30R_{\odot}$  from Zinn et al. (2019b) in an analysis using the APOKASC-2 first-ascent red giant sample and Gaia DR2 data. The systematic uncertainty in this case is not the full systematic uncertainty from that analysis, but rather just the systematic uncertainty arising from the Gaia DR2 zero point (1.3%), because otherwise the same asteroseismic parallax data were used (apart from small differences in the APOGEE DR14 and DR16 temperatures).

The shifts of up to 0.021 in  $a$  for Model 14 and Model 16 compared to Model 0 are to be expected because they both use the Kallinger et al. (2018) nonlinear scaling relations (Equation (3)), which may differ systematically from the APOKASC-2 radius scale described by Equation (2). Although the Kallinger et al. (2018) nonlinear scaling relations are calibrated to some of the same data used by the Pinsonneault et al. (2018) calibration, the methodologies differ. Indeed, one might expect a  $1\sigma$  systematic difference in  $a$  of 0.018, which includes the variation in the Gaia DR2 zero point (Zinn et al. 2019a), a 0.7% variation in the APOKASC-2 radius scale due to the calibration to open cluster masses (Pinsonneault et al. 2018), and an uncertainty of 1.1% due to possible variation in the nonlinear exponents,  $\kappa$  and  $\gamma$ , of Equation (3).

#### 4.3. Corrections to Gaia Parallaxes: The Constant Offset Term

I consider the local offset of  $c = -15 \pm 2 \mu\text{as}$  to be a conservative estimate of the mean deviation of parallaxes in the Kepler field from the parallax scale of quasars to which the  $Z_5$  model is tied. This is because the local offset is defined, consistent with the Gaia team’s  $Z_5$  model, at  $\nu_{\text{eff}} = 1.48 \mu\text{m}^{-1}$ , and so differences in the color trend in the parallax residuals would tend to shift  $c$ . For a fixed color trend in the residuals, the precise value of  $c$  will also depend on the choice of the pivot point, again, taken here to be  $\nu_{\text{eff}} = 1.48 \mu\text{m}^{-1}$ . Nevertheless, I do consistently find evidence across models for a local offset,  $c$ , of  $\approx -15 \mu\text{as}$ , even for Models 14–17, which prefer a  $\approx 100 \mu\text{as}$  less substantial color term than that of Model 0.

Perhaps more importantly, Models 14–17 all use the nonlinear scaling relations (Equation (3)) instead of the APOKASC-2  $f_{\Delta\nu}$  (Equation (2)) and prefer a different, more significant radius rescaling,  $a$  (Section 4.2). This suggests the fractional and additive corrections to parallaxes described by Equations (5) and (6) are well fit, even as there are correlations in the posteriors of  $c$  and  $a$  (Figure 1).

In spite of this conservative estimate, the best-fitting  $c$  is broadly consistent with the  $8.1 \mu\text{as}$  rms variation expected of Gaia parallaxes due to spatial correlations on scales the size of the Kepler field and larger inferred by the Kepler team using quasars (Lindgren et al. 2020b). For the analysis of spatial correlations on scales smaller than  $10^\circ$ , see Section 4.7.

#### 4.4. Corrections to Gaia Parallaxes: The Magnitude Term

As can be seen in Figure 3(f), a linear magnitude dependence is observed in the parallax residuals for  $11 \lesssim G < 13$ . Attempting to explain this trend with an explicit magnitude-dependent correction to the Gaia parallaxes is not strongly favored by the data: neither a model with the addition of a magnitude term (Model 3) nor a model with a magnitude term instead of a radius-rescaling term (Model 1) is strongly preferred over a model without a magnitude term (Model 0). Rather, this trend is well described by the radius-rescaling factor,  $a$  (Section 4.2), without the need for an explicit magnitude term,  $e$ . This is because the magnitude of a giant is correlated with its parallax, and residuals between the asteroseismic and Gaia parallax due to a fractional asteroseismic radius error will algebraically tend to increase in magnitude with increasing parallax.

As I do in interpretations of color-dependent adjustments to  $Z_5$  in Section 4.1, I adopt a conservative assumption that the  $Z_5$  model does not require adjustments in the absence of strong evidence. The preferred model therefore does not include  $e$ . Two other lines of evidence from independent work suggest that there is no need for refinements to  $Z_5$  that are linear in magnitude: (1) there is no evidence for a magnitude term from independent tests using Cepheids (Riess et al. 2021), and (2) the Yu et al. (2018) data prefer a magnitude term consistent with zero ( $e = 0.0 \pm 1.1 \mu\text{as mag}^{-1}$ ; Model 15). In short, I believe that the linear magnitude dependence in the parallax residuals of Figure 3(f) should be thought of instead as an error in the asteroseismic radius of  $\approx 0.5\%$ , which is the required level to explain the trend with magnitude in the absence of a magnitude term (Model 0).

It should also be noted that whatever refinements may be required of  $Z_5$  may not be captured by the model, because I assume a linear dependence in magnitude across a range of  $\sim 4$  mag; an attempt to make the magnitude trends of Equation (6) more granular by fitting two separate terms for  $G < 10.8$  and  $G \geq 10.8$  is strongly disfavored (Model 7 versus Model 0). By contrast, the  $Z_5$  model is more fine-grained, describing magnitude-dependent systematics with piecewise functions with four breakpoints ( $G = 10.8, 11.2, 11.8, 12.2$ ) within the magnitude range of the sample (Lindgren et al. 2020a). (The  $\Delta Z$  model in this analysis, however, does provide a more local measurement of color systematics than the  $Z_5$  model (Section 4.1).)

Apart from the small trend with magnitude seen in Figure 3(f), there is an abrupt shift in the parallax residuals at  $G \approx 11$ . There is no plausible astrophysical reason for why there should be a discontinuous parallax difference at  $G \approx 11$  and is instead indicative of shortcomings in the Gaia  $Z_5$  model, given that (1) this is the magnitude at which there is a window transition between WC0a and WC0b (Lindgren et al. 2020b), and that (2)  $G = 10.8$  is also a breakpoint in the magnitude-dependent terms of the  $Z_5$  model (thus motivating the choice for pivot point in Equation (6)). I model this with the  $c_2$  term, which is effectively a local offset just for the brightest stars in the sample ( $G < 10.8$ ). I find strong evidence for a nonzero value of  $c_2 = -15 \pm 3 \mu\text{as}$  (Model 8 versus Model 0), in the sense that corrected Gaia parallaxes for  $G < 10.8$  are too large.

EDR3 parallaxes are also found to be too large by  $-14 \pm 6 \mu\text{as}$  compared to photometric parallaxes from classical Cepheids with colors  $1.35 \mu\text{m}^{-1} < \nu_{\text{eff}} < 1.6 \mu\text{m}^{-1}$  and brighter than  $G \approx 11$  (Riess et al. 2021). Bhardwaj et al. (2021) find a similar offset of  $-25 \pm 5 \mu\text{as}$  compared to RR Lyrae ( $\nu_{\text{eff}} > 1.5 \mu\text{m}^{-1}$ ,  $G \lesssim 12$ ).

$c_2$  is also consistent to within  $2\sigma$  with the offset of  $+15 \pm 18 \mu\text{as}$  from eclipsing binaries ( $5 \lesssim G \lesssim 12$ ,  $\nu_{\text{eff}} > 1.5 \mu\text{m}^{-1}$ ; Stassun & Torres 2021). More recently, an analysis using photometric red clump parallaxes indicates an offset for  $G < 10.8$  with a magnitude of  $9.8 \pm 1 \mu\text{as}$  (Huang et al. 2021). An effect of  $\approx +10 \mu\text{as}$  in the opposite direction was noted when validating the  $Z_5$  model with LMC stars ( $G < 13$ ,  $\nu_{\text{eff}} > 1.7 \mu\text{m}^{-1}$ ; Lindegren et al. 2020a). Comparisons using the Washington Double Star Catalog (Mason et al. 2001) also showed a  $+10 \mu\text{as}$  offset in the opposite direction between the data and the  $Z_5$  model for stars  $G < 7$  (Fabricius et al. 2020).

One possible explanation for the bright-end parallax systematic I find here is that the  $Z_5$  model does not have the correct  $q_{00}$  coefficients, which are weights in the  $Z_5$  model that describe constant, additive corrections to EDR3 parallaxes at particular magnitude breakpoints, with linear ramps between adjacent breakpoints. The required increase in  $q_{00}$  of  $\approx 15 \mu\text{as}$  appears inconsistent with the statistical uncertainties for  $q_{00}$  coefficients for breakpoints  $G = 6.0, 10.8, 11.2$  that contribute to the  $Z_5$  model for the  $10 < G < 10.8$  range (Figure 11 of Lindegren et al. 2020a). However, it should be noted the bright-regime solution for  $Z_5$  is iterative, depending on (1) an intermediate solution bridging the quasar+LMC  $Z_5$  solution valid for  $G > 13$  and one that includes bright wide binaries down to  $G = 10$  and (2) a subsequent iterative solution that includes additional wide binaries with  $G < 6$ . This could plausibly cause systematic errors in the bootstrapped solution for  $G < 10.8$ , as noted by Lindegren et al. (2020a). Although an increase in  $q_{00}$  for  $G \lesssim 11$  would worsen the too-small blue LMC stars with  $G \lesssim 13$  noted by Lindegren et al. (2020a), there are too few stars with  $G \lesssim 11$  in Figure 19 of Lindegren et al. (2020a) to discern if the too-small problem actually exists for  $G \lesssim 11$  rather than only  $11 \lesssim G \lesssim 13$ . It is also plausible that the too-blue LMC stars are subject to their own systematics altogether unrelated to and unaffected by any  $c_2$  or indeed any other systematic identifiable with the sample: the too-small parallaxes occur for stars that have  $\nu_{\text{eff}} > 1.72 \mu\text{m}^{-1}$ , which is the color regime with no chromaticity calibration for five-parameter solutions and which is a regime not fitted with a linear color term in  $Z_5$ , but rather a constant of  $0.24 \times q_{10}$  (Lindegren et al. 2020a).

The best-fitting  $c_2$  term is shown in Figure 4, where black error bars indicate the parallax residuals after correction of the asteroseismic parallaxes by the radius-rescaling factor,  $a$ , and after removing residual color trends and removing a local offset with the  $c$  term, according to Equation (6) and the parameters of Model 0 in Table 1. The purple shaded region therefore represents the bright-end  $c_2$  adjustment to the  $Z_5$  model, which is the term for which I find the strongest evidence among all the terms in Equation (6). (The purple band in Figure 4 corresponds to the purple band in Figures 2 and 3.) Because this analysis is limited to a single  $10 \times 10 \text{ deg}^2$  area in sky coverage, it is conceivable that the  $c_2$  term could be specific to the ecliptic latitude of the Kepler field. However, given its concordance with a very similar term found using Cepheids distributed across the sky Riess et al. (2021) and red clump stars distributed across the sky (Huang et al. 2021), I believe that  $c_2$  is likely to be universal for  $G < 10.8$ .

#### 4.5. Comparison to Gaia DR2

As noted above, the difference between the asteroseismic parallaxes and the raw Gaia EDR3 parallaxes without applying

the  $Z_5$  correction is  $+22 \mu\text{as}$  in the sense that the EDR3 parallaxes are smaller. This is a significant improvement from the Gaia DR2 global zero point inferred for this red giant sample in Zinn et al. (2019a) of  $+53 \mu\text{as}$ . Some combination of the improved basic angle modeling with VBAC and photometric modeling incorporated into the astrometric solution procedure and the longer observation period in EDR3 compared to DR2 contributes to this systematics reduction.

Regarding the color- and magnitude-dependent terms in EDR3 compared to DR2, the  $e = -4.2 \pm 0.8 \mu\text{as mag}^{-1}$  magnitude term found in Zinn et al. (2019a) is in the same direction and of similar magnitude to the value of  $-2.6 \pm 0.9 \mu\text{as mag}^{-1}$  we find here for Model 1. Nevertheless, a nonzero  $e$  is not preferred by the EDR3 data (see Section 4.4). A color term, on the other hand, is significantly preferred by the EDR3 data, which I find to be larger in magnitude than the color term of  $d = -220 \pm 21 \mu\text{as } \mu\text{m}$  found by Zinn et al. (2019a) in Gaia DR2 parallaxes when using the same  $K_s$ -band bolometric correction adopted here. This difference may be partially caused by the different definition of  $\nu_{\text{eff}}$  in this work and Zinn et al. (2019a): in DR2, the data model included `astrometric_pseudocolour`, which was computed and defined analogously to the `pseudocolour` quantity in the EDR3 data model, which is now only provided for the six-parameter solutions. Indeed, adopting the DR2 `astrometric_pseudocolour` values as  $\nu_{\text{eff}}$  reduces the inferred  $d$  for EDR3 to  $\approx -270 \pm 20 \mu\text{as } \mu\text{m}$ , which is consistent within  $2\sigma$  with DR2. That the EDR3 and DR2 color terms are comparable suggests that neither the improvements in EDR3 to chromaticity corrections in the image parameter determination (Rowell et al. 2020) nor the  $Z_5$  model completely corrects color-dependent parallax systematics.

#### 4.6. Statistical Uncertainty in Gaia Parallaxes

In spite of nominally more than doubling the parallax precision for  $9 \lesssim G \lesssim 12$  in EDR3 compared to DR2 (Lindegren et al. 2020b), there are indications that EDR3 statistical parallax uncertainties are increasingly underestimated for brighter stars—Lindegren et al. (2020a) and Fabricius et al. (2020) note that the uncertainties appear to be underestimated by at least 30% in the  $G < 13$  regime. In an independent analysis using wide binaries, El-Badry et al. (2021) estimate that sources with no close companions of similar brightness have EDR3 parallax uncertainties underestimated by 20%–30% for  $G < 13$ .

For the fiducial analysis, I did not modify the nominal Gaia parallax or asteroseismic parallax uncertainties, setting  $k = g = 1$  (Model 0). Given that the  $\chi^2/\text{dof}$  for Model 0 is significantly smaller than unity (Table 1), I consider in Model 12 what  $k$  (rescaling of the Gaia parallax) and  $g$  (rescaling of the asteroseismic parallax) would be preferred by the model (Equations (4) and (7)). I infer that the Gaia parallax uncertainties are too small by  $22\% \pm 6\%$ , and also that asteroseismic parallax uncertainties are too large by  $31\% \pm 3\%$ .

Regarding the inferred overestimation of the asteroseismic parallaxes, I note that the APOKASC-2 asteroseismic uncertainties are estimated conservatively (Pinsonneault et al. 2018). The uncertainties were taken to be the observed scatter in the pipeline results for each star, imposing a lower bound of 0.9% and 0.4% in  $\nu_{\text{max}}$  and  $\Delta\nu$ , respectively. The rationale behind this approach is well motivated, i.e., so as to not allow unreasonably small uncertainties due to chance agreements among the pipeline measurements, but does impose an artificial

noise floor. The resulting statistical uncertainty estimates were seen to result in too-low chi-squared per degree of freedom in the mean mass of red giants in NGC 6791 and NGC 6819 of 0.6 and 0.8, confirming the conservative nature of the uncertainty estimates. The required deflation factor would leave uncertainties in  $\Delta\nu$  and  $\nu_{\max}$  still larger than the lower bound estimates of the intrinsic scatter in the  $\Delta\nu$  and  $\nu_{\max}$  parts of the red clump asteroseismic scaling relations of  $0.1\% \pm 0.2\%$  for  $\Delta\nu$  and  $0.7\% \pm 0.2\%$  for  $\nu_{\max}$  (Li et al. 2021).

Concerning the level of EDR3 parallax uncertainty underestimation, I confirm the results of Fabricius et al. (2020) and El-Badry et al. (2021), finding an average underestimation of  $22\% \pm 6\%$  in the Gaia parallaxes in the magnitude range  $9 \lesssim G \lesssim 13$  probed by the sample. I note that the underestimation effect appears to depend on magnitude (Fabricius et al. 2020; El-Badry et al. 2021), suggesting that  $k$  varies within the sample, which spans a range of approximately four magnitudes. I therefore corrected the Gaia parallax uncertainties according to the magnitude-dependent function of El-Badry et al. (2021) to infer if there were a need for further correction to the Gaia parallaxes. The resulting  $g$  (Model 12 in Table 1) is consistent with unity, which indicates both that (1) the approach in this analysis is sensitive to estimating both asteroseismic and Gaia parallax uncertainty corrections (a 30% inflation of the asteroseismic parallaxes is still inferred in this case, even as  $g = 1.02 \pm 0.04$ ) and that (2) the El-Badry et al. (2021) corrections perform well.

One can also compare how much of the Gaia uncertainty underestimation may be due to the spatial covariance estimated in Section 4.7. I estimate that the uncertainty in the mean Gaia parallax in the sample when including the spatial covariance of Equation (8) and Table 2 is 15% larger than the uncertainty from the reported EDR3 statistical uncertainties, which implies that  $\sim 1/2$  of the underestimation of the statistical uncertainties may be due to spatial covariance induced notionally by the scanning pattern of the Gaia satellite. As noted by both Fabricius et al. (2020) and El-Badry et al. (2021), there is a tendency for crowded regions to have more significantly underestimated parallax uncertainties than less crowded regions, which may be a contributing factor in addition to the variance induced by spatial correlations.

An additive correction to the Gaia parallax uncertainties—which could also equally be interpreted as an intrinsic scatter in the asteroseismic–Gaia parallax difference unexplained by the rest of the model—is not favored ( $s$  in Equation (7); Model 6 versus Model 0). In other words, the Gaia parallax uncertainties are well described by being fractionally underestimated rather than requiring additive corrections.

#### 4.7. Spatial Correlations in Gaia Parallaxes

In addition to pointing out the underestimation of statistical uncertainties in EDR3 parallaxes, the Gaia team quantifies systematic variations in parallax as a function of position on the sky induced by the scanning pattern of the satellite (Lindegren et al. 2020b). The present analysis extends the Gaia team’s analysis to smaller scales, redder colors, and brighter magnitudes compared to their estimate with faint, blue quasars. The operating principle behind the estimate provided here is that asteroseismic parallaxes are astrophysically expected to have no intrinsic correlation with position in the  $10 \times 10 \text{ deg}^2$  Kepler field, and, thus any spatial systematics in EDR3

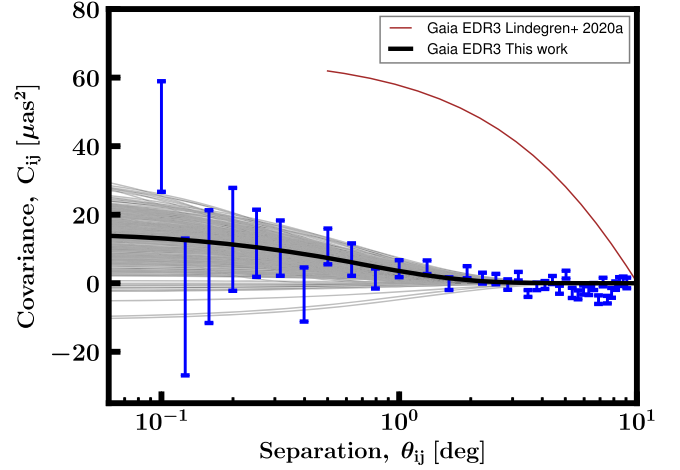


**Figure 5.** Parallax covariance for scales probed by the Kepler field ( $0.1 \lesssim \theta_{ij} \lesssim 10^\circ$ ), as inferred from the differences between asteroseismic and Gaia parallaxes after correcting according to  $Z_5$  and Equations (5) and (6) (blue error bars). The best-fitting model of the form Equation (8) with parameters according to Table 2 is shown as the black curve. Random draws for the best-fitting model parameters consistent with the covariance among the parameters are shown as gray curves. For comparison, a model of quasar parallax covariance from Lindegren et al. (2020b) found for fainter magnitudes ( $G > 17$ ) and for larger angular scales ( $\theta_{ij} \gtrsim 0.5^\circ$ ) is shown as the brown curve, less the expected large-scale covariance. See Section 4.7 for details.

parallaxes would manifest as spatially correlated differences between asteroseismic and EDR3 parallaxes.

In detail, the estimate of the spatial correlations in Gaia parallaxes follows Zinn et al. (2017).<sup>4</sup> I correct the Gaia parallaxes according to the  $Z_5$  prescription and also according to Model 0, further subtracting off any residuals by forcing the Gaia parallaxes to have the same mean parallax as the asteroseismic parallaxes. I then compute the covariance of the parallax difference  $\varpi_{\text{seis}} - \varpi_{\text{Gaia}}$ ,  $C_{ij} = \langle (\varpi_{\text{seis}} - \varpi_{\text{Gaia}})_i (\varpi_{\text{seis}} - \varpi_{\text{Gaia}})_j \rangle$  for pairs of stars,  $i$  and  $j$ , in bins of angular separation,  $\theta_{ij}$ , estimating the uncertainties in the covariance using from bootstrap sampling (Zinn et al. 2017).<sup>5</sup>

The resulting covariance at given angular scales are shown as error bars in Figure 5. A positive value indicates a correlation between parallaxes at a given angular separation, and a negative value indicates an anticorrelation. If there were no spatial correlations in the Gaia parallaxes, the covariance would be zero.

I then fit the covariance with the model of Equation (8) via MCMC, adopting uncertainties on each binned covariance point as shown in Figure 5. The resulting model is shown as a solid black curve in Figure 5. The gray curves are random draws of the best-fitting model, according to the covariance among the best-fitting parameters, as estimated from the MCMC chains.

I show for reference the Gaia team covariance model from Lindegren et al. (2020b) as the solid brown curve. I note that the Gaia model is fit to large scales  $\theta_{ij} \gtrsim 0.5^\circ$ , and so I only show the Lindegren et al. (2020b) model in that regime. I have

<sup>4</sup> Following Zinn et al. (2019b), I do not consider the uncertainty in the estimation due to “cosmic variance”: the finite sampling of the spatial correlations due to looking only at the Kepler field. I do, however, take into account edge effects through bootstrap sampling, according to Zinn et al. (2017).

<sup>5</sup> Whereas Zinn et al. (2017) computed a binned Pearson correlation coefficient, I compute here the covariance, which differs by a factor of the variance in the parallax difference.



also subtracted the variance inferred on scales larger than the Kepler field of  $76 \mu\text{as}^2$  (Lindgren et al. 2020b) to make it more comparable to the results of this analysis, though I expect residual differences to remain (see below).

As can be seen in Figure 5 and from the best-fitting parameters in Table 2, the systematic covariance floor at the smallest scales is  $4.0 \pm 1 \mu\text{as}$ , which corresponds to  $35\% \pm 10\%$  of the statistical uncertainty of  $\varpi_{\text{Gaia}}$  in the sample. Already at a low level on small scales, the covariance becomes negligible on scales larger than a few degrees.

In the overlap region of  $0^\circ.5 \lesssim \theta_{ij} \lesssim 10^\circ$  between the covariance estimated here and that estimated by Lindgren et al. (2020b) using quasars, the quasar covariance model is markedly larger than the covariances of the Kepler field (brown versus black curves in Figure 5). This may be indicative of smaller spatial systematics in the  $G < 13$  regime compared to the  $G > 17$  regime probed by quasars or may signal variation in the small-scale systematics across the sky. Note that there will be an offset between the covariance estimated here using the Kepler field and the covariance inferred from quasars because the latter has contributions from scales larger than  $10^\circ$ . As noted above, I attempt to correct for this difference by removing  $8.7 \mu\text{as}$  in quadrature from the quasar covariance, which is the estimated rms scatter in quasar parallaxes on scales larger than  $7^\circ$  (Lindgren et al. 2020b); a large-scale rms scatter of  $\approx 11 \mu\text{as}$  would be required to reconcile the quasar covariance and the Kepler field covariance at  $0^\circ.5$ , which is also consistent with the Kepler field local offset I find of  $c = -15 \pm 2 \mu\text{as}$  (Section 4.3). I also note that the quasar parallaxes were not corrected for the  $Z_5$  model, which will leave spatial systematics due to the ecliptic latitude-dependent zero-point terms modeled with  $Z_5$ , and which could help explain the  $\approx 2 \mu\text{as}$  larger rms scatter required to match the quasar and Kepler field covariances. I note that Fardal et al. (2021) find that the level of spatial correlation in Gaia DR2 parallaxes increases by a factor of 6 between  $G = 13$  and  $G = 20$ . Under the assumption that this magnitude dependence is preserved in EDR3 spatial correlations, this would be another reason to expect a larger spatial covariance among quasars than I find here.

The spatial covariance found in this work would be expected to be in better agreement with the Gaia team’s estimates of the covariance using the LMC than those using quasars because there are no contributions from large-scale variations. Additionally, the LMC members are more comparable in magnitude to the sample here. Indeed, the estimate from Lindgren et al. (2020b) of a systematic uncertainty of  $6.9 \mu\text{as}$  for  $0^\circ.1 \lesssim \theta_{ij} \lesssim 4^\circ.5$  accords better with the present estimate of  $4 \pm 1 \mu\text{as}$  at the smallest scales, keeping in mind the larger systematic expected of the LMC estimate due to not correcting the parallaxes using  $Z_5$ .

I stress that the spatial covariance estimation procedure used here will not be sensitive to any average parallax systematic that persists over the entire Kepler field of view, because I correct the parallaxes according to Equation (6). However, the local offset term that I find,  $c = -15 \pm 2 \mu\text{as}$ , is a conservative estimate of what sort of average offset the astroseismic and Gaia parallaxes have, averaged over the whole Kepler field (see Section 4.3). This is consistent with the expected rms of  $8.1 \mu\text{as}$  on scales larger than  $10^\circ$  using quasars (Lindgren et al. 2020b). Studies making use of the small-scale covariance as described by Equation (8) and Table 2 would therefore be

advised that the large-scale contributions to the covariance may well be larger than the small-scale ones that are available using the Kepler field.

## 5. Concluding Remarks

I have compared Gaia EDR3 parallaxes with five-parameter solutions to parallaxes derived from knowledge of the temperature, bolometric flux, and astroseismic radius for more than 2000 first-ascent red giant branch stars in the Kepler field, and conclude the following:

1. The  $Z_5$  zero-point model (Lindgren et al. 2020a) brings Gaia EDR3 parallaxes into agreement with astroseismic parallaxes to an average of  $\approx 2 \mu\text{as}$  before any adjustments to  $Z_5$  or astroseismic parallaxes for the regime  $10.8 \leq G < 13$ ,  $1.4 \mu\text{m}^{-1} \lesssim \nu_{\text{eff}} \lesssim 1.5 \mu\text{m}^{-1}$  (purple band in Figure 2).
2. I find strong evidence that the  $Z_5$  zero-point model overcorrects parallaxes for  $9 \lesssim G \lesssim 11$ , such that corrected parallaxes are too large by  $15 \mu\text{as} \pm 3 \mu\text{as}$  (purple band in Figure 4(f)), consistent with the findings for even brighter Cepheids distributed across the sky ( $6 \lesssim G \lesssim 10$ ; Riess et al. 2021).
3. I identify a significant color dependence to the astroseismic–Gaia parallax residuals of  $-300 \pm 25 \mu\text{as} \mu\text{m}$  for  $G \gtrsim 11$  and  $1.4 \mu\text{m}^{-1} \lesssim \nu_{\text{eff}} \lesssim 1.5 \mu\text{m}^{-1}$ , of which  $\sim 100 \mu\text{as} \mu\text{m}$  may plausibly be attributed to astroseismic parallax systematic uncertainties. If this color term were due to unmodeled behavior in  $Z_5$ , there is reason to believe it may have an ecliptic latitude dependence.
4. After removing the aforementioned color term from the astroseismic–Gaia parallax residuals and after adjusting  $Z_5$  according to an additive  $-15 \pm 3 \mu\text{as}$  offset for  $G < 10.8$ , the Gaia EDR3 and astroseismic parallaxes agree to within a constant offset of  $c = -15 \pm 2 \mu\text{as}$ . The latter may be interpreted as a conservative estimate of the large-scale variation in the parallax zero point, given its dependence on color trends, and is broadly consistent with the Gaia team’s estimates of spatially correlated parallax variations on scales larger than the Kepler field.
5. Gaia EDR3 parallax statistical uncertainties in the  $9 \lesssim G \lesssim 13$ ,  $1.4 \mu\text{m}^{-1} \lesssim \nu_{\text{eff}} \lesssim 1.5 \mu\text{m}^{-1}$  regime probed by the sample are underestimated by  $22\% \pm 6\%$ , consistent with estimates from the Gaia team (Fabricius et al. 2020) and in good agreement with independent analysis using wide binaries (El-Badry et al. 2021).
6. The spatial correlations in Gaia EDR3 parallaxes on the scales probed by the Kepler field ( $\lesssim 10^\circ$ )—described by Equation (8) with parameters in Table 2—agree broadly with those inferred by Lindgren et al. (2020b) to within an additive constant due to correlations on scales larger than the Kepler field. These spatial correlations incur a  $\approx 4 \mu\text{as}$  systematic parallax uncertainty on angular scales less than  $\approx 0^\circ.1$ , falling to below a  $\approx 0.1 \mu\text{as}$  level on scales larger than  $\approx 5^\circ$  (Figure 5).

The zero point in EDR3 is not expected to be significantly different in the next installment of Data Release 3 scheduled in 2022, because the next complete astrometric solution will only be done for Gaia DR4. At that time, further reduction in the parallax zero point is expected in part due to the reversal of the Gaia satellite’s precession (Lindgren et al. 2020b). Until such time, further characterization of the EDR3  $Z_5$  model would be



fruitful, particularly to definitively constrain any color adjustments needed of it and to validate it as a function of ecliptic latitude.

I am grateful to Adam Riess for encouraging, productive conversations and instructive comments. I would also like to thank Ruth Angus and the Center for Computational Astrophysics for providing office space during the COVID-19 pandemic. Thanks go especially to the Gaia team for their revolutionary work. I am supported by an NSF Astronomy and Astrophysics Postdoctoral Fellowship under award AST-2001869.

This work has made use of data from the European Space Agency (ESA) mission Gaia (<https://www.cosmos.esa.int/gaia>), processed by the Gaia Data Processing and Analysis Consortium (DPAC, <https://www.cosmos.esa.int/web/gaia/dpac/consortium>). Funding for the DPAC has been provided by national institutions, in particular the institutions participating in the Gaia Multilateral Agreement.

Funding for the Sloan Digital Sky Survey IV has been provided by the Alfred P. Sloan Foundation, the U.S. Department of Energy Office of Science, and the Participating Institutions.

SDSS-IV acknowledges support and resources from the Center for High Performance Computing at the University of Utah. The SDSS website is [www.sdss.org](http://www.sdss.org).

SDSS-IV is managed by the Astrophysical Research Consortium for the Participating Institutions of the SDSS Collaboration including the Brazilian Participation Group, the Carnegie Institution for Science, Carnegie Mellon University, Center for Astrophysics—Harvard & Smithsonian, the Chilean Participation Group, the French Participation Group, Instituto de Astrofísica de Canarias, The Johns Hopkins University, Kavli Institute for the Physics and Mathematics of the Universe (IPMU)/University of Tokyo, the Korean Participation Group, Lawrence Berkeley National Laboratory, Leibniz Institut für Astrophysik Potsdam (AIP), Max-Planck-Institut für Astronomie (MPIA Heidelberg), Max-Planck-Institut für Astrophysik (MPA Garching), Max-Planck-Institut für Extraterrestrische Physik (MPE), National Astronomical Observatories of China, New Mexico State University, New York University, University of Notre Dame, Observatório Nacional/MCTI, The Ohio State University, Pennsylvania State University, Shanghai Astronomical Observatory, United Kingdom Participation Group, Universidad Nacional Autónoma de México, University of Arizona, University of Colorado Boulder, University of Oxford, University of Portsmouth, University of Utah, University of Virginia, University of Washington, University of Wisconsin, Vanderbilt University, and Yale University.

This publication makes use of data products from the Two Micron All Sky Survey, which is a joint project of the University of Massachusetts and the Infrared Processing and Analysis Center/California Institute of Technology, funded by the National Aeronautics and Space Administration and the National Science Foundation.

*Software:* asfgrid (Sharma & Stello 2016), NumPy (Walt et al. 2011), pandas (McKinney 2010), Matplotlib (Hunter 2007), IPython (Pérez & Granger 2007), SciPy (Virtanen et al. 2020), isoclassify (Huber et al. 2017; Berger et al. 2020), corner (Foreman-Mackey 2016).

## ORCID iDs

Joel C. Zinn  <https://orcid.org/0000-0002-7550-7151>

## References

- Ahumada, R., Prieto, C. A., Almeida, A., et al. 2020, *ApJS*, **249**, 3
- Arenou, F., Luri, X., Babusiaux, C., et al. 2018, *A&A*, **616**, A17
- Belkacem, K., Goupil, M. J., Dupret, M. A., et al. 2011, *A&A*, **530**, A142
- Berger, T. A., Huber, D., van Saders, J. L., et al. 2020, *AJ*, **159**, 280
- Bhardwaj, A., Rejkuba, M., de Grijs, R., et al. 2021, *ApJ*, **909**, 200
- Blanton, M. R., Bershadsky, M. A., Abolfathi, B., et al. 2017, *AJ*, **154**, 28
- Bobylev, V. V. 2019, *AstL*, **45**, 10
- Borucki, W. J., Koch, D., Basri, G., et al. 2010, *Sci*, **327**, 977
- Brewer, L. N., Sandquist, E. L., Mathieu, R. D., et al. 2016, *AJ*, **151**, 66
- Brogaard, K., Bruntt, H., Grundahl, F., et al. 2011, *A&A*, **525**, A2
- Brogaard, K., Vandenberg, D. A., Bruntt, H., et al. 2012, *A&A*, **543**, A106
- Brown, T. M., Gilliland, R. L., Noyes, R. W., & Ramsey, L. W. 1991, *ApJ*, **368**, 599
- Butkevich, A. G., Klioner, S. A., Lindegren, L., Hobbs, D., & van Leeuwen, F. 2017, *A&A*, **603**, A45
- Chan, V. C., & Bovy, J. 2020, *MNRAS*, **493**, 4367
- Chaplin, W. J., Houdek, G., Appourchaux, T., et al. 2008, *A&A*, **485**, 813
- Davies, G. R., Lund, M. N., Miglio, A., et al. 2017, *A&A*, **598**, L4
- De Ridder, J., Molenberghs, G., Eyser, L., & Aerts, C. 2016, *A&A*, **595**, L3
- El-Badry, K., Rix, H.-W., & Heintz, T. M. 2021, arXiv:2101.05282
- Fabrizius, C., Luri, X., Arenou, F., et al. 2020, arXiv:2012.06242
- Fardal, M. A., van der Marel, R., del Pino, A., & Sohn, S. T. 2021, *AJ*, **161**, 58
- Foreman-Mackey, D. 2016, *JOSS*, **1**, 24
- Gaia Collaboration, Brown, A. G. A., Vallenari, A., et al. 2012, arXiv:2012.01533
- Gaia Collaboration, Brown, A. G. A., Vallenari, A., et al. 2016, *A&A*, **595**, A2
- Gaia Collaboration, Brown, A. G. A., Vallenari, A., et al. 2018, *A&A*, **616**, A1
- García Pérez, A. E., Allende Prieto, C., Holtzman, J. A., et al. 2016, *AJ*, **151**, 144
- González Hernández, J. I., & Bonifacio, P. 2009, *A&A*, **497**, 497
- Groenewegen, M. A. T. 2018, *A&A*, **619**, A8
- Grundahl, F., Clausen, J. V., Hardis, S., & Frandsen, S. 2008, *A&A*, **492**, 171
- Guggenberger, E., Hekker, S., Basu, S., & Bellinger, E. 2016, *MNRAS*, **460**, 4277
- Gunn, J. E., Siegmund, W. A., Mannery, E. J., et al. 2006, *AJ*, **131**, 2332
- Hall, O. J., Davies, G. R., Elsworth, Y. P., et al. 2019, *MNRAS*, **486**, 3569
- Holtzman, J. A., Hasselquist, S., Shetrone, M., et al. 2018, *AJ*, **156**, 125
- Holtzman, J. A., Shetrone, M., Johnson, J. A., et al. 2015, *AJ*, **150**, 148
- Huang, Y., Yuan, H., Beers, T. C., & Zhang, H. 2021, *ApJL*, **901**, L5
- Huber, D., Stello, D., Bedding, T. R., et al. 2009, *CoAst*, **160**, 74
- Huber, D., Zinn, J., Bojsen-Hansen, M., et al. 2017, *ApJ*, **844**, 102
- Hunter, J. D. 2007, *CSE*, **9**, 90
- Jao, W.-C., Henry, T. J., Riedel, A. R., et al. 2016, *ApJL*, **832**, L18
- Jeffries, M. W., Jr., Sandquist, E. L., Mathieu, R. D., et al. 2013, *AJ*, **146**, 58
- Kallinger, T., Beck, P. G., Stello, D., & García, R. A. 2018, *A&A*, **616**, A104
- Kass, R. E., & Raftery, A. E. 1995, *J. Am. Stat. Assoc.*, **90**, 773
- Khan, S., Miglio, A., Mosser, B., et al. 2019, *A&A*, **628**, A35
- Kjeldsen, H., & Bedding, T. R. 1995, *A&A*, **293**, 87
- Kounkel, M., Covey, K., Suárez, G., et al. 2018, *AJ*, **156**, 84
- Layden, A. C., Tiede, G. P., Chaboyer, B., Bunner, C., & Smitka, M. T. 2019, *AJ*, **158**, 105
- Leggett, S. K., Bergeron, P., Subasavage, J. P., et al. 2018, *ApJS*, **239**, 26
- Leung, H. W., & Bovy, J. 2019, *MNRAS*, **489**, 2079
- Li, Y., Bedding, T. R., Stello, D., et al. 2021, *MNRAS*, **501**, 3162
- Lindegren, L., Bastian, U., Biermann, M., et al. 2020a, arXiv:2012.01742
- Lindegren, L., Hernández, J., Bombrun, A., et al. 2018, *A&A*, **616**, A2
- Lindegren, L., Klioner, S. A., Hernández, J., et al. 2020b, arXiv:2012.03380
- Lindegren, L., Lammers, U., Bastian, U., et al. 2016, *A&A*, **595**, A4
- Majewski, S. R., Wilson, J. C., Hearty, F., Schiavon, R. R., & Skrutskie, M. F. 2010, in IAU Symp. 265, Chemical Abundances in the Universe: Connecting First Stars to Planets, ed. K. Cunha, M. Spite, & B. Barbuy (Cambridge: Cambridge Univ. Press), 480
- Mamajek, E. E., Prsa, A., Torres, G., et al. 2015, arXiv:1510.07674
- Marconi, M., Molinaro, R., Ripepi, V., et al. 2021, *MNRAS*, **500**, 5009
- Marrese, P. M., Marinoni, S., Fabrizio, M., & Altavilla, G. 2019, *A&A*, **621**, A144
- Mason, B. D., Wycoff, G. L., Hartkopf, W. I., Douglass, G. G., & Worley, C. E. 2001, *AJ*, **122**, 3466
- McKinney, W. 2010, in Proc. 9th Python in Science Conf., ed. S. van der Walt & J. Millman (Austin, TX: SciPy), 56

- Melnik, A. M., & Dambis, A. K. 2020, [Ap&SS](#), **365**, 112
- Michalik, D., Lindegren, L., & Hobbs, D. 2015, [A&A](#), **574**, A115
- Muhie, T. D., Dambis, A. K., Berdnikov, L. N., Kniazev, A. Y., & Grebel, E. K. 2021, [MNRAS](#), **502**, 4074
- Muraveva, T., Delgado, H. E., Clementini, G., Sarro, L. M., & Garofalo, A. 2018, [MNRAS](#), **481**, 1195
- Nidever, D. L., Holtzman, J. A., Allende Prieto, C., et al. 2015, [AJ](#), **150**, 173
- Paxton, B., Bildsten, L., Dotter, A., et al. 2011, [ApJS](#), **192**, 3
- Paxton, B., Cantiello, M., Arras, P., et al. 2013, [ApJS](#), **208**, 4
- Paxton, B., Marchant, P., Schwab, J., et al. 2015, [ApJS](#), **220**, 15
- Paxton, B., Schwab, J., Bauer, E. B., et al. 2018, [ApJS](#), **234**, 34
- Paxton, B., Smolec, R., Schwab, J., et al. 2019, [ApJS](#), **243**, 10
- Pérez, F., & Granger, B. E. 2007, [CSE](#), **9**, 21
- Pinsonneault, M. H., Elsworth, Y. P., Tayar, J., et al. 2018, [ApJS](#), **239**, 32
- Riess, A. G., Casertano, S., Yuan, W., et al. 2018, [ApJ](#), **861**, 126
- Riess, A. G., Casertano, S., Yuan, W., et al. 2021, [ApJL](#), **908**, L6
- Rodrigues, T. S., Girardi, L., Miglio, A., et al. 2014, [MNRAS](#), **445**, 2758
- Rowell, N., Davidson, M., Lindegren, L., et al. 2020, arXiv:2012.02069
- Sandquist, E. L., Mathieu, R. D., Brogaard, K., et al. 2013, [ApJ](#), **762**, 58
- Schlafly, E. F., & Finkbeiner, D. P. 2011, [ApJ](#), **737**, 103
- Schönrich, R., McMillan, P., & Eyer, L. 2019, [MNRAS](#), **487**, 3568
- Schwarz, G. 1978, [AnSta](#), **6**, 461
- Sharma, S., & Stello, D. 2016, Asfgrid: Asteroseismic Parameters for a Star, Version 0.0.5., Astrophysics Source Code Library, ascl:1603.009
- Sharma, S., Stello, D., Bland-Hawthorn, J., Huber, D., & Bedding, T. R. 2016, [ApJ](#), **822**, 15
- Skrutskie, M. F., Cutri, R. M., Stiening, R., et al. 2006, [AJ](#), **131**, 1163
- Stassun, K. G., & Torres, G. 2016, [ApJL](#), **831**, L6
- Stassun, K. G., & Torres, G. 2021, [ApJL](#), **907**, L33
- Sun, Q., Deliyannis, C. P., Twarog, B. A., Anthony-Twarog, B. J., & Steinhauer, A. 2020, [AJ](#), **159**, 246
- Tayar, J., Claytor, Z. R., Huber, D., & van Saders, J. 2020, arXiv:2012.07957
- Torra, F., Castañeda, J., Fabricius, C., et al. 2020, arXiv:2012.06420
- Torres, G. 2010, [AJ](#), **140**, 1158
- Ulrich, R. K. 1986, [ApJL](#), **306**, L37
- Virtanen, P., Gommers, R., Oliphant, T. E., et al. 2020, [NatMe](#), **17**, 261
- Walt, S. v. d., Colbert, S. C., & Varoquaux, G. 2011, [CSE](#), **13**, 22
- White, T. R., Bedding, T. R., Stello, D., et al. 2011, [ApJ](#), **743**, 161
- Wilson, J. C., Hearty, F. R., Skrutskie, M. F., et al. 2019, [PASP](#), **131**, 055001
- Yalyaliev, L. N., Chemel, A. A., Glushkova, E. V., Dambis, A. K., & Klinichev, A. D. 2018, [AstBu](#), **73**, 335
- Yu, J., Huber, D., Bedding, T. R., et al. 2018, [ApJS](#), **236**, 42
- Zinn, J. C., Huber, D., Pinsonneault, M. H., & Stello, D. 2017, [ApJ](#), **844**, 166
- Zinn, J. C., Pinsonneault, M. H., Huber, D., & Stello, D. 2019a, [ApJ](#), **878**, 136
- Zinn, J. C., Pinsonneault, M. H., Huber, D., et al. 2019b, [ApJ](#), **885**, 166